Acta Pharmaceutica Sinica B 2026;16(8):5148−5167

Chinese Pharmaceutical Association
Institute of Materia Medica, Chinese Academy of Medical Sciences

Acta Pharmaceutica Sinica B

www.elsevier.com/locate/apsb
www.sciencedirect.com

ORIGINAL ARTICLE

Novel circUnc79 regulates morphine-induced reward memory *via* the miR-149-3p/EAAT2 axis and glutamatergic plasticity

Xixi Yang[a,b,†], Feifei Gao[a,b,†], Zhuojin Yang[a,b], Dongyu Yu[a,b], Jie Chen[a,b], Zhen Yao[c], Qi Liao[c], Jingsi Yang[a,b], Junlin Liu[a,b], Boyuan Gu[a,b], Yuxiang Zhang[a,b,*], Chunxia Yan[a,b,c,*]

[a]*College of Forensic Medicine, Key Laboratory of National Health Commission for Forensic Medicine, Xi'an Jiaotong University Health Science Center, Xi'an 710061, China*
[b]*Bio-evidence Sciences Academy, Science and Technology Innovation Harbour of Western China, Xi'an Jiaotong University, Xi-xian 712000, China*
[c]*National Narcotics Laboratory Shaanxi Branch, Xi-xian 712000, China*

Received 25 August 2025; received in revised form 10 December 2025; accepted 3 March 2026

KEY WORDS

Circular RNAs;
Morphine;
Opioid addiction;
Reward memory;
Synaptic plasticity;
Medial prefrontal cortex;
EAAT2;
miR-149-3p

Abstract Opioid addiction is driven by maladaptive reward memory, yet its molecular underpinnings remain poorly understood. Circular RNAs (circRNAs) have emerged as key regulators of neuroplasticity, but their roles in addiction-related memory remain unclear. Here, we identify circUnc79, a neuron-enriched and synaptically localized circRNA, as a critical modulator of morphine reward memory in the medial prefrontal cortex (mPFC). In the morphine-induced conditioned place preference (CPP) model, circUnc79 expression is dynamically downregulated during cue-induced memory retrieval. Gain- and loss-of-function experiments demonstrate that circUnc79 bidirectionally regulates the acquisition and persistence of morphine reward memory, without affecting locomotion, anxiety-like behavior, social interaction, or sucrose reward. Mechanistically, circUnc79 acts as a competing endogenous RNA for miR-149-3p, thereby relieving its repression of excitatory amino acid transporter 2 (EAAT2, encoded by *Slc1a2*). Elevated neuronal EAAT2 enhances presynaptic glutamate reuptake and recycling, supporting reward memory encoding. Manipulation of miR-149-3p produces opposite behavioral and synaptic effects, supporting the functional relevance of this regulatory axis. These findings reveal a circUnc79/miR-149-3p/EAAT2 pathway that regulates synaptic plasticity underlying opioid reward memory and highlight circUnc79 as a potential therapeutic target for opioid use disorders.

*Corresponding authors.
E-mail addresses: yuxiangzhang@xjtu.edu.cn (Yuxiang Zhang), yanchunxia@xjtu.edu.cn (Chunxia Yan).
[†]These authors made equal contributions to this work.
Peer review under the responsibility of Chinese Pharmaceutical Association and Institute of Materia Medica, Chinese Academy of Medical Sciences.

https://doi.org/10.1016/j.apsb.2026.06.004

1. Introduction

Opioid use disorder (OUD) remains a major global health challenge, characterized by compulsive drug-seeking behavior, high relapse rates, and persistent vulnerability to drug-associated cues[1]. A central obstacle in addiction treatment is the enduring nature of drug-associated memories, which drive craving and relapse upon re-exposure to drug-paired contexts[2]. These maladaptive memories are formed and maintained through neuroplastic adaptations within corticolimbic circuits, particularly in the medial prefrontal cortex (mPFC), a key region involved in reward processing, decision-making, and executive control[3]. At the molecular level, drug-induced neuroplasticity engages complex transcriptional and post-transcriptional mechanisms that regulate synaptic structure and function. While previous studies have largely focused on protein-coding genes and epigenetic regulation, emerging evidence highlights a critical role for non-coding RNAs in addiction-related plasticity[4].

Circular RNAs (circRNAs), a class of covalently closed and exonuclease-resistant non-coding RNAs, are highly enriched in the brain[5]. Their stability, evolutionary conservation, and cell-type-specific expression suggest important roles in supporting long-term synaptic adaptations associated with addictive behaviors[6]. One well-characterized function of circRNAs is to act as competing endogenous RNAs (ceRNAs), sequestering microRNAs (miRNAs) and thereby modulating downstream gene expression[7]. This mechanism has been implicated in multiple neuropsychiatric disorders, including depression, schizophrenia, and substance use disorders[8,9]. For example, circTmeff-1 in the nucleus accumbens promotes morphine craving by sponging miR-541-5p and miR-6934-3p, thereby upregulating two synapse-related proteins, vesicle-associated membrane protein 1 (VAMP1) and neurofascin (NFASC)[9]. Despite these advances, the precise role of circRNAs in opioid addiction, particularly during the retrieval of drug-associated memories, remains poorly understood.

Disruption of glutamatergic homeostasis is a core feature of addiction, with altered glutamate signaling observed across multiple classes of drugs, including opioids[10]. Excitatory amino acid transporter 2 (EAAT2), encoded by *Slc1a2*, plays a central role in extracellular glutamate clearance and recycling, thereby maintaining synaptic glutamate homeostasis[11]. Although EAAT2 is predominantly expressed in astrocytes, emerging evidence suggests that neuronal EAAT2 may also contribute to the regulation of presynaptic glutamate dynamics and synaptic plasticity[12−14]. Astrocytic EAAT2 is essential for preventing excitotoxicity[15], whereas neuronal EAAT2 has been proposed to fine-tune synaptic efficacy by modulating local glutamate recycling[13]. However, whether neuronal EAAT2 is subject to circRNA-mediated regulation in the context of opioid addiction remains unclear.

Our previous transcriptomic analyses of the mPFC following morphine exposure revealed widespread dysregulation of circRNAs and genes associated with synaptic plasticity[16,17]. Building on these findings, we identified circUnc79 (circBase ID: mmu_circ_0000411), a neuron-enriched circRNA derived from the *Unc79* gene, as a key regulator of morphine-induced reward memory in the mPFC. Using integrated molecular, behavioral, and morphological approaches, we demonstrate that circUnc79 modulates morphine-induced synaptic plasticity through a miR-149-3p/EAAT2-dependent pathway. This regulatory axis promotes neuroadaptive changes characterized by enhanced mPFC excitability and presynaptic glutamate recycling, thereby supporting the encoding and retrieval of morphine reward memory.

Collectively, our findings identify circUnc79 as a previously unrecognized post-transcriptional regulator of synaptic remodeling in opioid addiction and suggest its potential as a therapeutic target for modulating drug-associated memories and reducing relapse risk in OUD.

2. Materials and methods

2.1. Animals and drugs

Male C57BL/6J mice (8 weeks old, 20−25 g) were obtained from the Medical Experimental Animal Center of Xi'an Jiaotong University (Xi'an, China). Mice were housed under standard conditions (22 ± 2 °C, 12-h light/dark cycle) with ad libitum access to food and water. All procedures were approved by the Institutional Animal Care and Use Committee of Xi'an Jiaotong University (No. 2022-1174). Morphine was purchased from the National Institutes for Food and Drug Control of China and was dissolved in sterile 0.9% saline. Mice received morphine (10 mg/kg, i.p.), while control mice received an equal volume of saline.

2.2. Cell lines and authentication

CATH.a (ATCC CRL-11179) and Neuro-2a (ATCC CCL-131) cells were obtained from Cobioer (Nanjing, China) and Pricella (Wuhan, China), respectively. All cell lines were authenticated by the suppliers and confirmed to be mycoplasma-free before use.

2.3. Conditioned place preference (CPP) paradigm

The CPP paradigm was conducted as previously described, with minor modifications[16]. The apparatus consisted of three chambers with distinct cues. Briefly, on Day 0, mice were allowed to explore freely for 15 min. During conditioning (Days 1−5), mice were conditioned with either saline or morphine (10 mg/kg, i.p.). Post-test was conducted on Day 6, followed by a retrieval test on Day 13 after a 7-day interval. Behavior was recorded using SMART 3.0 (Panlab SL, Barcelona, Spain). CPP score was calculated as the difference in time spent in the morphine-paired chamber *versus* the saline-paired chamber. Additional behavioral tests, including elevated plus maze, open field test, Y-maze, novel object recognition, three-chamber social interaction, and sucrose preference tests, were described in the Supporting Information Methods. After testing, mice were sacrificed, and mPFC tissues were dissected according to the Paxinos and Franklin atlas coordinates and snap-frozen in liquid nitrogen.

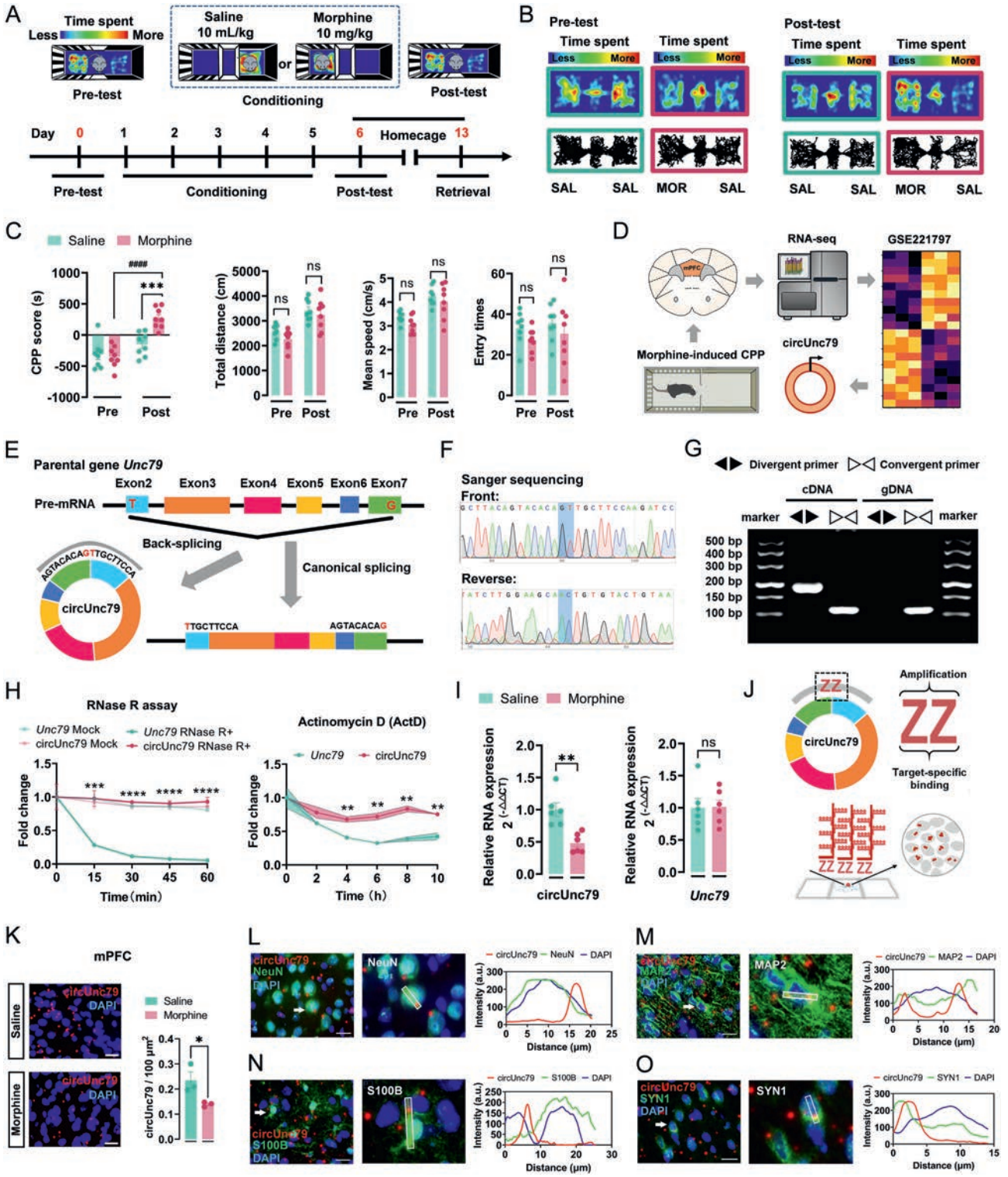

Figure 1 Identification and characterization of circUnc79 as a morphine reward memory-associated circRNA in the mPFC. (A) Timeline of the CPP paradigm. Mice underwent baseline preference assessment (Day 0), conditioning with morphine (10 mg/kg, i.p.) or saline (Days 1−5), post-test (Day 6), 7-day home-cage withdrawal, and retrieval test (Day 13). (B, C) Representative locomotor trajectories and heat maps (B) and quantitative CPP scores and locomotor parameters (C) ($n = 8$) (two-way ANOVA followed by Bonferroni *post hoc* test). (D) RNA-seq workflow for circUnc79 identification. (E−G) circUnc79 biogenesis schematic (E), Sanger sequencing of the back-splice junction (F), and divergent PCR validation (G). (H) Characterization of circUnc79 stability. Left: time−course analysis of RNase R digestion. Total RNA was treated with RNase R (3 U/μg) for the indicated time points (0, 15, 30, 45, and 60 min). Right: transcription inhibition assay using Actinomycin D (10 μg/mL). The time-dependent changes in RNA levels revealed a longer half-life of circUnc79 compared to linear *Unc79* ($n = 3$) (Student's *t*-test). (I) Downregulation of circUnc79, but not linear *Unc79*, in the mPFC after CPP ($n = 6$) (Student's *t*-test). (J−K) BaseScope probe design (J) and *in*

2.4. RNA extraction and quantitative reverse transcription PCR (RT-qPCR)

Total RNA was extracted from the mouse mPFC using SteadyPure Universal RNA Extraction Kit (Accurate Biotechnology, Changsha, China) according to the manufacturer's instructions, and quantified by NanoDrop 2000 spectrophotometer (Thermo Fisher, Waltham, MA, USA). For mRNA and circRNA, 1 μg of RNA was reverse-transcribed using the Hifair III 1st Strand cDNA Synthesis SuperMix (Yeasen Biotechnology, Shanghai, China). For miRNA, 500 ng of RNA was reverse-transcribed using either poly(A)-tailing (Accurate Biotechnology, Changsha, China) or stem-loop (Vazyme Biotech, Nanjing, China) methods. Quantitative PCR was performed using Hieff qPCR SYBR Green Master Mix (Yeasen Biotechnology, Shanghai, China) on a CFX96 Real-Time PCR System (Bio-Rad, Hercules, CA, USA). Primers were synthesized by Tsingke Biotechnology (Beijing, China). Relative RNA expression was calculated using the $2^{-\Delta\Delta Ct}$ method. GAPDH was used as the internal control for mRNAs and circRNAs, while U6 served as the reference for miRNA quantification. Sequences of all primers are listed in Supporting information Table S1.

2.5. RNA stability and degradation assays

RNase R digestion was performed to assess circUnc79 stability. Briefly, total RNA (2.5 μg) was incubated with or without RNase R (3 U/μg, Geneseed Biotech, Guangzhou, China) at 37 °C for the indicated time points (0, 15, 30, 45, and 60 min), followed by heat inactivation (70 °C, 10 min) and RT-qPCR analysis. For transcription inhibition assays, Neuro-2a cells were treated with Actinomycin D (ActD, 10 μg/mL) and collected at the indicated time points (0, 2, 4, 6, 8, and 10 h). Total RNA was extracted using TRIzol and analyzed by RT-qPCR.

2.6. circRNA validation by PCR and sanger sequencing

Divergent and convergent primers were designed to validate the circular structure of candidate circRNAs. PCR amplification was performed using 2 × Phusion High-Fidelity PCR Master Mix (New England Biolabs, Ipswich, MA, USA) with cDNA or genomic DNA as templates under standard conditions. PCR products were resolved on 2% agarose gels containing Ultra GelRed (Vazyme Biotech, Nanjing, China) in 1 × TAE buffer, mixed with 6 × DNA loading buffer (Thermo Fisher Scientific, Waltham, MA, USA), and separated alongside a DNA marker. Electrophoresis was conducted at 100 V for 30 min, and gel images were captured using a ChemiDoc XRS + imaging system (Bio-Rad, Hercules, CA, USA) and analyzed with Image Lab software. PCR products of the expected size were purified and sequenced by Sanger sequencing. Sequence traces were analyzed with SnapGene software, and back-splice junctions were confirmed by detection of head-to-tail junction sequences characteristic of circRNAs.

2.7. Cell culture, transfection, and lentiviral transduction

Cells were cultured in Dulbecco's modified Eagle's medium (DMEM; Gibco, Grand Island, NY, USA) supplemented with 10% fetal bovine serum and 1% penicillin/streptomycin at 37 °C in a humidified incubator with 5% CO_2. For transient transfection, miR-149-3p mimics or inhibitors (Tsingke Biotechnology, Beijing, China) were introduced using Lipofectamine 2000 (Invitrogen, Carlsbad, CA, USA) in Opti-MEM according to the manufacturer's instructions. Cells were harvested 48 h after transfection for subsequent analyses. For stable modulation of circUnc79, lentiviral vectors for overexpression (OE) or knockdown (KD) were obtained from GeneChem (Shanghai, China; see Supporting information Table S2). Cells were infected at a multiplicity of infection (MOI) of 10 with transduction enhancer (HiTransG P, GeneChem, Shanghai, China), and the medium was replaced after 12 h. Stable cells were selected with puromycin (2 μg/mL for Neuro-2a and 4 μg/mL for CATH.a) for 1 week, and transduction efficiency was verified by RT-qPCR.

2.8. BaseScope in situ hybridization and co-localization analysis

BaseScope assays (Advanced Cell Diagnostics, ACD, Newark, CA, USA) were performed to detect circUnc79 expression in mouse mPFC sections and Neuro-2a cells according to the manufacturer's instructions. Briefly, fresh-frozen brain tissues were embedded in O.C.T. compound (Sakura Finetek, Torrance, CA, USA), sectioned at 10 μm using a cryostat CM1950 (Leica, Wetzlar, Germany), and mounted onto slides. Sections were fixed with 4% paraformaldehyde, dehydrated, and pretreated with RNAscope reagents, including hydrogen peroxide, target retrieval reagent, and Protease IV (ACD). A specific probe targeting the back-splice junction of circUnc79 (Probe-BA-Mm-Unc79-circRNA-E7E2-Junc-C1, ACD) was hybridized at 40 °C, followed by signal amplification and detection using Fast Red substrate (ACD). Nuclei were counterstained with DAPI. Images were acquired using an AxioScope five microscope (ZEISS, Oberkochen, Germany) and analyzed with ImageJ. Negative and positive controls were performed using a scrambled probe (BaseScope Probe-BA-DapB-1zz, ACD) and a housekeeping probe (BaseScope Probe-BA-Mm-Ppib-1zz, ACD), respectively.

For co-localization analysis, BaseScope was combined with immunofluorescence using the Integrated Co-Detection Workflow (ACD). Sections were incubated with primary antibodies against NeuN (1:100, Proteintech, Wuhan, China), S100B, Iba1, and Olig2 (1:100, Abways, Shanghai, China), as well as MAP2, SYN1, and PSD95 (1:100, Proteintech, Wuhan, China), followed by Alexa Fluor 488- or 594-conjugated secondary antibodies (1:300, Proteintech, Wuhan, China). Neuro-2a cells cultured on chamber slides (LABSELECT, Beijing, China) were processed similarly. Images were acquired and analyzed as described above.

2.9. Stereotactic injection of adeno-associated virus (AAV) into the mPFC

AAV vectors (Supporting information Table S3) were stereotaxically injected into the mPFC using a 7100 automated stereotactic system (RWD Life Science, Shenzhen, China). Mice were anesthetized with isoflurane (4% for induction and 1.5%−2% for

situ hybridization (ISH) confirmation of decreased circUnc79 (red) in the mPFC (K). Scale bar = 20 μm ($n = 3$) (Student's *t*-test). (L−O) Cell-type specificity and subcellular localization of circUnc79. Representative images showing co-localization of circUnc79 (red) with (L) NeuN, (M) MAP2, (N) S100B, or (O) SYN1 (green). Nuclei were stained with DAPI (blue). Scale bars = 20 μm. Data are presented as mean ± SEM. $^{*}P < 0.05$, $^{**}P < 0.01$, $^{***}P < 0.001$, $^{****}P < 0.0001$; $^{\#\#\#\#}P < 0.0001$; ns, not significant.

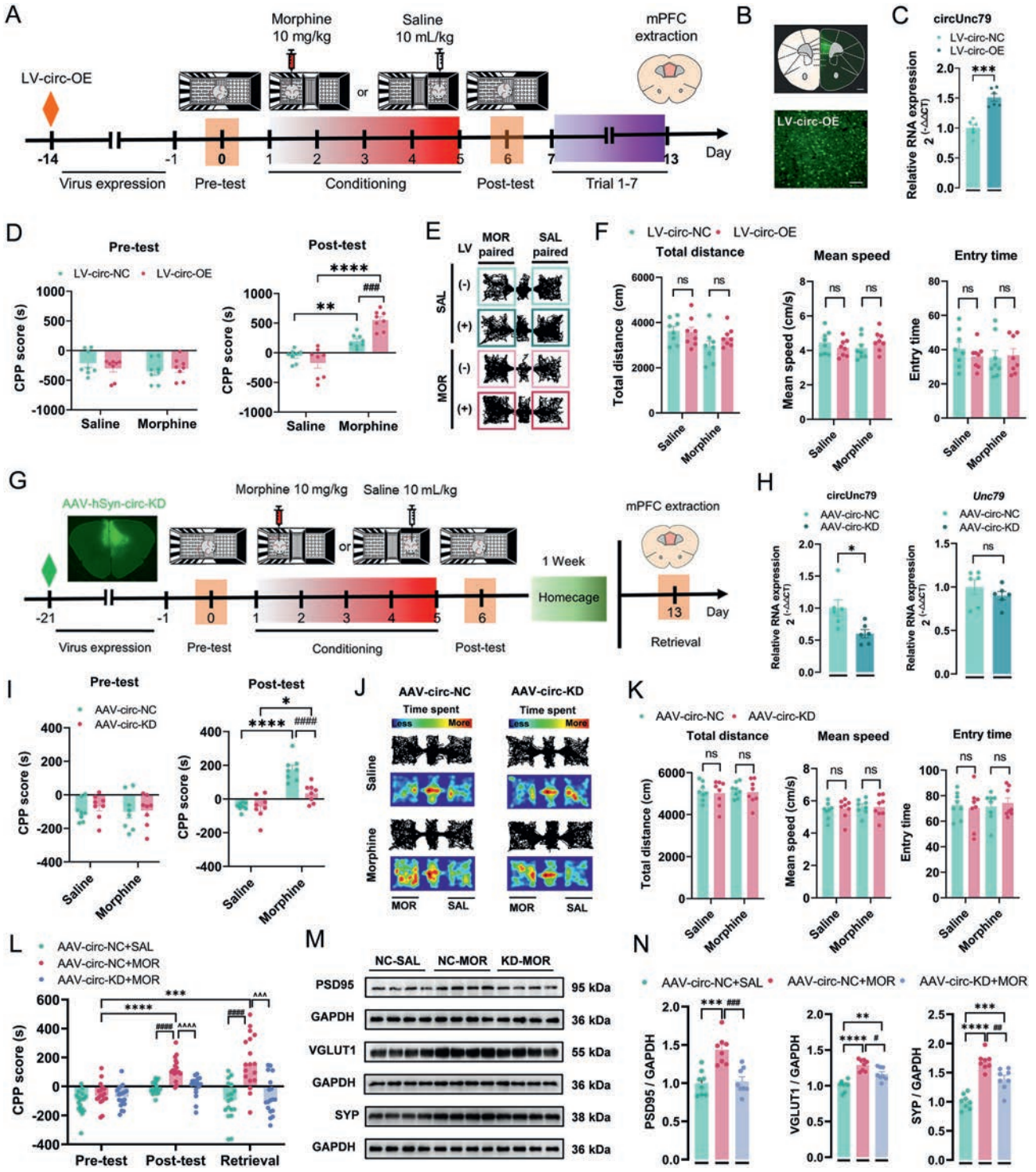

Figure 2 Bidirectional modulation of morphine-induced reward memory by mPFC circUnc79. (A) Experimental timeline: LV-circ-OE or control lentivirus was injected bilaterally into the mPFC two weeks before pre-test (Day 0), followed by morphine/saline conditioning (Days 1−5), post-test (Day 6), and retrieval tests (Days 7−13). (B) Schematic coronal section showing injection coordinates and fluorescence verification of mPFC-specific transduction. Scale bars = 500 μm (top), 100 μm (bottom). (C) RT-qPCR validation of circUnc79 overexpression efficiency (n = 6) (Student's t-test). (D−F) Effect of circUnc79 overexpression on morphine-induced CPP scores and locomotor parameters (n = 8) (two-way ANOVA followed by Bonferroni post-hoc test). (G) Experimental timeline: AAV-circ-KD was delivered into mPFC neurons three weeks before pre-test (Day 0), followed by morphine/saline conditioning (Days 1−5) and behavioral tests (Days 6 and 13). (H) RT-qPCR validation of AAV-mediated circUnc79 knockdown; linear *Unc79* transcripts remained unchanged (n = 6) (Student's t-test). (I−K) Morphine-induced CPP scores (I), representative trajectory and heat maps (J), and locomotor parameters (K) following circUnc79 knockdown (n = 8) (two-way ANOVA followed by Bonferroni *post hoc* test). (L) CPP scores during post-test and retrieval phases across knockdown and control groups (n = 18) (two-way ANOVA followed by Bonferroni *post hoc* test). (M, N) Expression levels of synapse-associated proteins following

maintenance, RWD Life Science, Shenzhen, China) and placed in a stereotaxic frame. A burr hole was drilled at the target coordinates (AP +1.98 mm, ML ±0.30 mm, DV −2.3 mm from bregma), and virus was delivered at 0.1 μL/min using a microsyringe (Hamilton Company, Reno, NV, USA). The needle was left in place for 10 min before slow withdrawal. Mice were sutured and allowed to recover under standard postoperative care. Injection accuracy was confirmed histologically, and mice recovered for 3 weeks before further experiments.

2.10. Dual-luciferase reporter assay

Wild-type (WT) or mutant (MUT) pmirGLO reporter constructs containing predicted miR-149-3p binding sites in circUnc79 or the *Slc1a2* (EAAT2) 3′ UTR were generated based on TargetScan and miRanda predictions and verified by Sanger sequencing. HEK-293T cells were cultured in DMEM supplemented with 10% fetal bovine serum and co-transfected with reporter plasmids and miR-149-3p mimics or negative control using Lipofectamine 2000 (Thermo Fisher Scientific, Waltham, MA, USA). After 48 h, luciferase activity was measured using a Dual-Luciferase Reporter Assay System (Yeasen Biotechnology, Shanghai, China). Firefly luciferase activity was normalized to *Renilla* luciferase activity.

2.11. RNA-binding protein immunoprecipitation (RIP) assay

RIP assays were performed using an RNA Immunoprecipitation Kit (Bersinbio, Guangzhou, China) to examine interactions among circUnc79, miR-149-3p, and EAAT2. Neuro-2a cells were lysed, and lysates were incubated with magnetic beads conjugated to an anti-Argonaute-2 (AGO2) antibody (4 μg/IP, Abcam, Cambridge, UK), with IgG as a negative control. RNA−protein complexes were immunoprecipitated, and the associated RNA was extracted for RT-qPCR analysis.

2.12. Western blotting

Western blotting was performed as described previously[18]. Proteins from mouse brain tissues or cultured cells were extracted using RIPA lysis buffer containing protease and phosphatase inhibitors and centrifuged to remove debris. Protein concentrations were determined using a BCA assay. Equal amounts of protein were separated by SDS-PAGE and transferred onto PVDF membranes (Merck Millipore, Burlington, MA, USA). Membranes were blocked with 5% skim milk and incubated with primary antibodies overnight at 4 °C, followed by HRP-conjugated secondary antibodies (Proteintech, Wuhan, China) for 1 h at room temperature. Bands were visualized using ECL substrate (DiNing, Beijing, China) and imaged with a ChemiDoc XRS + system (Bio-Rad, Hercules, CA, USA). Primary antibody details were listed in Supporting information Table S4.

2.13. Synaptosome isolation

Synaptosomes were isolated from mouse mPFC using the Minute Synaptosome Isolation Kit (Invent Biotechnologies, Plymouth, MN, USA) according to the manufacturer's protocol. Tissues were homogenized in buffer A using the supplied filter cartridge and centrifuged to remove debris. The resulting suspension was sequentially processed with buffer B and buffer C, followed by differential centrifugation to enrich the synaptosome fraction. The final synaptosome pellet was collected, resuspended, and stored at −80 °C until further use. Protein concentration was determined using a BCA assay. Synaptosome purity was verified by Western blotting using synaptic markers, including NMDAR1, NMDAR2A, NMDAR2B, GluR2, PSD-95, and VGLUT1.

2.14. Golgi-Cox staining and morphometric analysis

Neuronal morphology and dendritic spine density were assessed using Golgi-Cox staining. Brain tissues were immersed in staining solution for 14 days, then transferred to protective solution for 7 days. Coronal sections (150 μm) were prepared using a vibratome VT1200S (Leica, Wetzlar, Germany) and processed according to standard protocols. Images were acquired under a light microscope (Teksqray, Shenzhen, China) at 40× magnification and analyzed using ImageJ (NIH, Bethesda, MD, USA). For each group ($n = 4$), 15 intact pyramidal neurons in the mPFC were analyzed. Dendritic complexity was assessed by Sholl analysis (5 μm intervals, 10−120 μm from soma). Spine density was calculated as spines per 10 μm dendrite, and classified into thin, stubby, mushroom, and filopodium types. Analyses were performed in a blinded manner with ≥20 dendritic branches per group.

2.15. Transmission electron microscopy (TEM)

Mice were perfused with 0.25% glutaraldehyde and 4% paraformaldehyde in phosphate buffer (0.1 mol/L, pH 7.4). The mPFC was dissected into small tissue blocks (1 mm^3), fixed in 2.5% glutaraldehyde at 4 °C, and post-fixed in 1% osmium tetroxide. Samples were dehydrated, embedded in epoxy resin, and polymerized at 60 °C. Ultrathin sections (70 nm) were stained with uranyl acetate and lead citrate, and imaged using a transmission electron microscope (H-7650, Hitachi, Tokyo, Japan) at 80 kV. Synaptic ultrastructure was analyzed using Image-Pro Plus software.

2.16. Fiber photometry for calcium dynamics and glutamate fluctuations

Fiber photometry was performed to monitor in *vivo* calcium and glutamate signals using a system R820 (RWD Life Science, Shenzhen, China). Sensors (GCaMP7f, jRGECO1a, iGluSnFR3.v857) were delivered into the mPFC, followed by implantation of an optical fiber cannula (400 μm core, 0.39 NA, $L = 3$ mm, RWD Life Science, Shenzhen, China). After 3 weeks, recordings were conducted during CPP testing. Excitation at 470 nm (GCaMP7f and iGluSnFR3.v857) or 560 nm (jRGECO1a) was applied, with 410 nm as an isosbestic control. Signals were recorded and analyzed using multichannel fiber photometry software (RWD Life Science). Data are expressed as $\Delta F/F$.

2.17. Statistical analysis

Statistical analyses were performed using GraphPad Prism (GraphPad, USA). Data are presented as mean ± standard error of the mean (SEM).

circUnc79 knockdown in morphine-conditioned mice ($n = 4$) (one-way ANOVA followed by Bonferroni *post hoc* test). Data are presented as mean ± SEM. $^{*}P < 0.05$, $^{**}P < 0.01$, $^{***}P < 0.001$, $^{****}P < 0.0001$; $^{\#}P < 0.05$, $^{\#\#}P < 0.01$, $^{\#\#\#}P < 0.001$, $^{\#\#\#\#}P < 0.0001$; $^{\wedge\wedge}P < 0.001$, $^{\wedge\wedge\wedge\wedge}P < 0.0001$; ns, not significant.

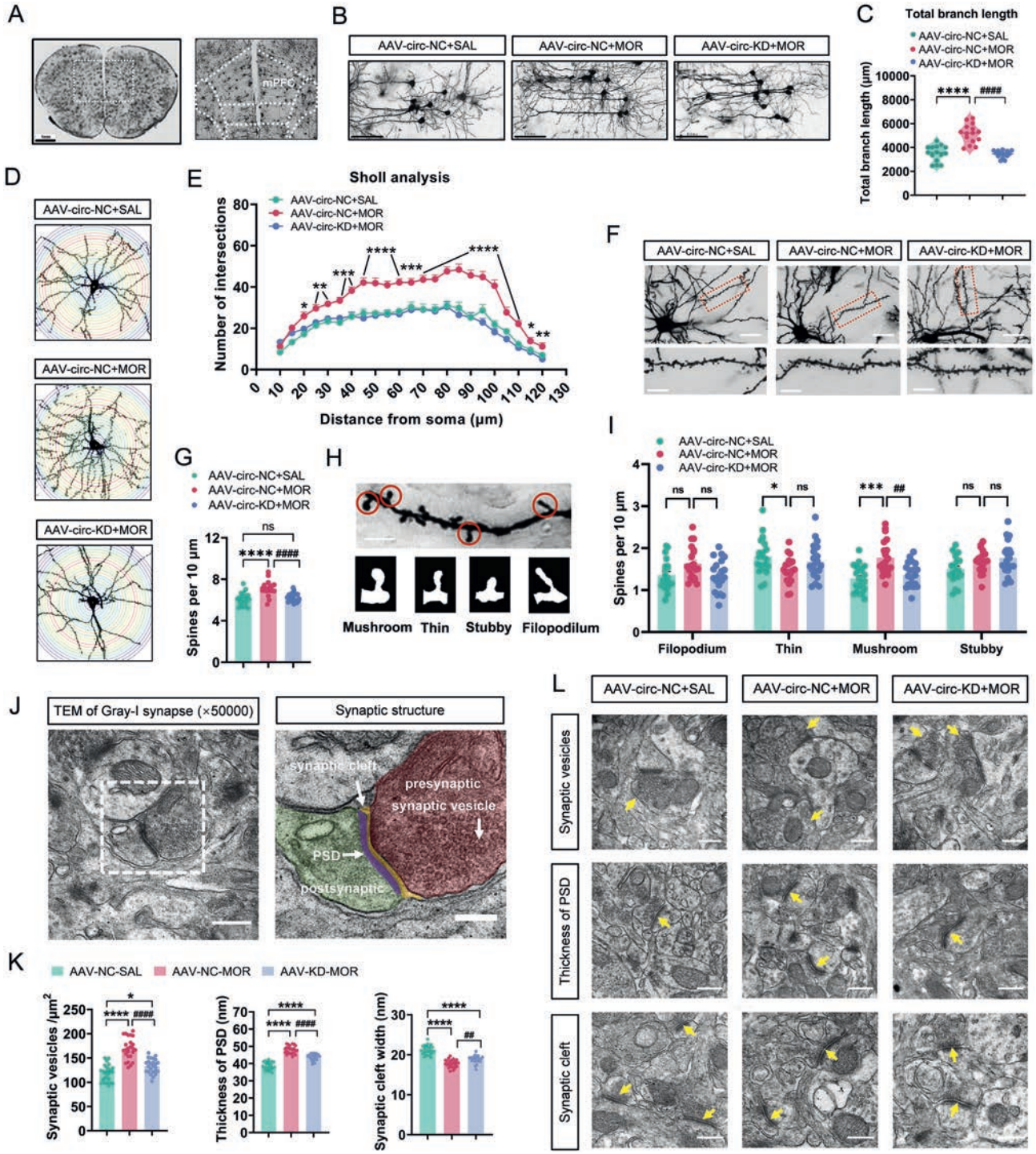

Figure 3 CircUnc79-dependent synaptic remodeling during morphine reward memory. (A) Coronal section of mPFC showing Golgi-impregnated neuronal architecture. Scale bar = 1 mm. (B) Representative pyramidal neurons in mPFC layer II/III. Scale bar = 100 μm. (C) Total dendritic branch length quantification. Morphine significantly increased branch length, which was attenuated by circUnc79 knockdown. (D) Sholl analysis using concentric circles (5 μm intervals, 10−120 μm radius) to quantify dendritic arborization complexity. (E) Sholl intersection profile showing morphine-enhanced dendritic complexity and its normalization by circUnc79 knockdown. Radial distance from the soma (*x*-axis) *vs.* intersections per shell (*y*-axis) ($n = 15$). (F) Representative images of secondary dendritic branches. Scale bar = 25 μm (overview), 10 μm (spine detail). (G) Dendritic spine density quantification (spines/10 μm). (H) Morphological classification of dendritic spines: mushroom, thin, stubby, and filopodium subtypes. Scale bar = 5 μm. (I) Morphine-induced shift in dendritic spine subtypes was rescued by circUnc79 knockdown ($n = 20$). (J) Representative TEM images of asymmetric Gray's type I synapse highlighting ultrastructural regions Presynaptic terminals (red), PSD (purple), and synaptic clefts (yellow). Scale bars = 400 nm (left), 200 nm (right). (K) Morphine conditioning increased presynaptic vesicle density and PSD thickness while reducing synaptic cleft width. These effects were reversed by circUnc79 knockdown. (L) TEM images of

Two-group comparisons used unpaired two-tailed Student's *t*-tests. Multiple comparisons were analyzed by one- or two-way ANOVA with Bonferroni *post hoc* tests. Exact tests and *P* values are provided in the Source Data. $P < 0.05$ was considered statistically significant.

3. Results

3.1. CircUnc79 in the mPFC mediated cue-associated morphine reward memory

Morphine-induced conditioned place preference (CPP) was established in mice, as indicated by a significant increase in dwell time and CPP scores in the morphine group compared to saline controls during the post-test ($P < 0.001$), without changes in locomotor activity (Fig. 1A−C). This reward memory remained stable during the retrieval test on Day 13 (Supporting information Fig. S1), providing a suitable time point for transcriptomic analysis. RNA sequencing of mPFC tissue harvested after the retrieval test (GSE221797)[16] identified circUnc79 (circBase ID: mmu_circ_0000411) as a differentially expressed circRNA candidate (Fig. 1D). Derived from the parental gene *Unc79* (*Unc79* homolog, NALCN channel complex subunit), circUnc79 is formed *via* back-splicing of exon two to exon 7 (Fig. 1E). Its circular structure was validated by divergent primer PCR and Sanger sequencing, which confirmed the specific back-splicing junction (Fig. 1F and G) and demonstrated its evolutionary conservation across mammalian species (Supporting information Fig. S2). Furthermore, circUnc79 exhibited greater stability compared to its linear counterpart, demonstrating resistance to RNase R digestion and actinomycin D-induced transcription inhibition (Fig. 1H).

Notably, quantitative expression analysis revealed that circUnc79 was significantly downregulated in the mPFC following morphine-induced CPP ($P < 0.01$), whereas linear *Unc7*9 mRNA levels remained unaltered (Fig. 1I). This downregulation was consistent across different morphine doses (5, 10, and 20 mg/kg; Supporting information Fig. S3) and exhibited regional specificity, with no changes observed in the NAc, Hipp, VTA, or BLA (Supporting information Fig. S4). Crucially, circUnc79 levels remained stable in home-cage mice receiving chronic morphine in the absence of contextual pairing (Supporting information Fig. S5). These findings suggested that circUnc79 was a spatially restricted, memory-associated molecular signature, distinct from a generalized pharmacological response to morphine.

At the cellular level, BaseScope *in situ* hybridization demonstrated a broad distribution of circUnc79 across mPFC laminae, confirming its downregulation in CPP mice (Fig. 1J and K, Supporting information Fig. S6). Co-localization assays revealed that circUnc79 was predominantly enriched in neurons, displaying clear overlap with MAP2 and SYN1 (Fig. 1L−O, Supporting information Fig. S7−S9). Quantitative analysis revealed that neurons showed the highest expression level (55.46 ± 3.32%), significantly exceeding that observed in astrocytes (21.28 ± 3.87%), microglia (17.70 ± 2.28%), and oligodendrocytes (12.27 ± 1.69%). Consequently, neurons constituted the majority (78.45%) of the total circUnc79-positive population (Supporting information Figs. S10 and S11). Further characterization indicated that circUnc79 was preferentially enriched in excitatory glutamatergic neurons (with minimal overlap with GAD67; Supporting information Fig. S12) and localized to presynaptic compartments, with 71.26 ± 4.23% of circUnc79 puncta co-localizing with SYN1 compared to only 24.09 ± 1.72% with the postsynaptic marker PSD-95 (Supporting information Fig. S13).

3.2. Bidirectional modulation of morphine reward memory by circUnc79 in the mPFC

To investigate the functional role of circUnc79 in morphine-induced reward memory, lentiviral vectors (LV-circ-OE) were bilaterally injected into the mPFC to overexpress circUnc79 (Fig. 2A). Fluorescence microscopy confirmed robust expression confined to the mPFC (Fig. 2B). Consistently, RT-qPCR analysis showed that circUnc79 levels were markedly elevated in the LV-circ-OE group compared with controls ($P < 0.001$), validating the efficiency of the overexpression strategy (Fig. 2C).

Behaviorally, circUnc79 overexpression significantly potentiated morphine reward memory. Two-way ANOVA revealed a significant Drug × Virus interaction ($F = 22.08$, $P = 0.0003$), indicating that the effects of viral manipulation were dependent on drug treatment. While viral intervention did not alter behavior in saline-treated mice ($P > 0.05$), *post hoc* analysis demonstrated that LV-circ-OE + MOR mice exhibited significantly elevated CPP scores compared to morphine-treated controls ($t = 4.193$, $P = 0.0005$; Fig. 2D−F), suggesting enhanced morphine-induced CPP. Moreover, circUnc79 overexpression significantly impaired extinction learning, as evidenced by persistently elevated CPP scores across multiple extinction sessions (Supporting information Fig. S14).

Based on its neuronal localization, we performed neuron-specific knockdown using an hSyn-driven AAV-shRNA (Fig. 2G), which selectively reduced circUnc79 ($P < 0.05$) without affecting linear *Unc7*9 mRNA (Fig. 2H). Two-way ANOVA revealed significant main effects for Drug ($F = 44.74$, $P < 0.0001$) and Virus ($F = 15.33$, $P = 0.0016$), as well as a critical Drug × Virus interaction ($F = 9.721$, $P = 0.0076$). *Post hoc* comparisons confirmed that knockdown of circUnc79 significantly reduced morphine-induced preference ($t = 4.894$, $P < 0.0001$) while not affecting saline baseline behavior ($P > 0.05$; Fig. 2I−K). Temporal analysis showed that circUnc79 knockdown attenuated CPP scores during both the acquisition phase ($P < 0.0001$) and the retrieval phase ($P < 0.001$; Fig. 2L and Supporting information Fig. S15), suggesting that circUnc79 contributed to both the formation and expression of morphine reward memory. Moreover, knockdown facilitated extinction learning and prevented morphine priming-induced reinstatement of drug-seeking behavior (Supporting information Fig. S16). This intervention did not affect locomotor activity (Supporting information Fig. S17), anxiety, spatial memory, social cognition, and natural reward processing (Supporting information Fig. S18), indicating behavioral specificity.

To explore molecular correlates, we assessed synapse-associated proteins in the mPFC following the retrieval test. Western blot analysis revealed that morphine conditioning induced robust upregulation of key synaptic markers, including

synaptic ultrastructure. Yellow arrows indicated analyzed regions: synaptic vesicles (top), PSD (middle), synaptic cleft (bottom). Scale bar = 400 nm ($n = 25$). Data are presented as mean ± SEM. $^{*}P < 0.05$, $^{**}P < 0.01$, $^{***}P < 0.001$, $^{****}P < 0.0001$; $^{\#\#}P < 0.01$, $^{\#\#\#\#}P < 0.0001$; ns, not significant (one-way ANOVA followed by Bonferroni *post hoc* test).

PSD95, VGLUT1, and synaptophysin (SYP). Importantly, circUnc79 knockdown normalized these morphine-induced changes, restoring synaptic protein levels toward baseline (Fig. 2M and N). Together, these results suggested circUnc79 as a critical and specific regulator of morphine reward memory, likely through the modulation of synaptic plasticity-related pathways.

3.3. CircUnc79 knockdown reversed morphine-induced synaptic remodeling

Building on the established role of circUnc79 in modulating synapse-associated proteins during morphine memory retrieval, we conducted neuromorphological analysis to investigate its effects on synaptic plasticity in the mPFC. Golgi staining was performed to assess dendritic architecture in morphine-conditioned mice (Fig. 3A and B). Morphine exposure significantly enhanced dendritic arborization, characterized by increased total dendritic branch length ($P < 0.0001$ *vs*. saline; Fig. 3C) and increased dendritic complexity in Sholl analysis, as indicated by a greater number of dendritic intersections at distances of 10−120 μm from the soma (Fig. 3D and E). Notably, circUnc79 knockdown reversed these morphine-induced morphological changes, restoring dendritic complexity and length toward baseline levels (Fig. 3C−E). Dendritic spine analysis further identified synapse-specific plasticity modulated by circUnc79. Morphine conditioning increased overall spine density ($P < 0.0001$ *vs.* saline), preferentially expanding mature mushroom-type spines ($P < 0.001$) while reducing immature thin spines ($P < 0.05$) (Fig. 3F−I). Knockdown of circUnc79 attenuated this subtype-specific redistribution, restoring total spine density toward control levels.

Transmission electron microscopy (TEM) revealed ultrastructural synaptic changes following morphine-associated memory retrieval (Fig. 3J−L). Presynaptic terminals exhibited a 1.42-fold increase in synaptic vesicle density ($P < 0.0001$ *vs.* saline), suggesting increased neurotransmitter release capacity. This effect was attenuated by circUnc79 knockdown ($P < 0.0001$ *vs.* morphine) (Fig. 3K). Concurrently, morphine induced a 1.24-fold thickening of postsynaptic densities (PSDs) ($P < 0.0001$), which was partially reversed by circUnc79 knockdown ($P < 0.0001$ *vs.* morphine). Additionally, morphine-associated memory retrieval reduced synaptic cleft width ($P < 0.0001$), whereas circUnc79 knockdown restored cleft width ($P < 0.01$ *vs.* morphine). Collectively, these findings demonstrated that circUnc79 contributed to the consolidation of morphine-associated memory by coordinately modulating presynaptic vesicle pools and postsynaptic structural integrity.

3.4. CircUnc79 knockdown reversed morphine-induced neuronal hyperexcitability

Since circUnc79 knockdown reversed both presynaptic and postsynaptic remodeling, we next assessed whether it affected neuronal excitability in the mPFC during reward memory retrieval. *In vivo* fiber photometry was used to monitor calcium transients in mPFC neurons during morphine-induced CPP (Fig. 4A and B). Fluorescence imaging confirmed the co-expression of jRGECO1a and circUnc79-targeting AAVs, validating signal specificity (Fig. 4C).

Time-locked fiber photometry recordings during CPP were performed using dual-wavelength illumination (560 nm signal; 410 nm reference) to calculate normalized $\Delta F/F$ (Fig. 4D). Morphine-conditioned mice exhibited neuronal hyperactivity upon drug-paired chamber entry (Fig. 4E), characterized by a 12.87-fold increase in calcium transient amplitude ($\Delta F/F$) compared with saline ($P < 0.0001$) (Fig. 4F and G). Analysis of calcium event kinetics showed that memory retrieval significantly increased calcium event frequency ($P < 0.0001$) while decreasing individual event duration ($P < 0.001$) compared to saline controls (Supporting information Fig. S19). Remarkably, circUnc79 knockdown significantly reversed these morphine-induced alterations across all parameters, restoring neuronal activity toward baseline levels and suggesting its role in sustaining context-dependent excitability.

Event-triggered heatmaps further revealed that morphine elicited sustained high-amplitude activation specifically in the drug-paired context. This chamber-specific excitability was normalized following circUnc79 silencing, with activation patterns resembling those of saline controls (Fig. 4H). These findings demonstrated that circUnc79 contributed to morphine-associated reward memory by sustaining synaptic and neuronal excitability changes in response to contextual drug cues.

3.5. Multimodal validation of the circUnc79/miR-149-3p/EAAT2 ceRNA regulatory axis

To elucidate the molecular mechanism underlying circUnc79's regulation of drug-seeking behavior, we systematically validated the ceRNA network through multimodal approaches. We employed a dual-transcriptomic strategy integrating morphine-induced mPFC RNA-seq (GSE221797) with ONT-seq validation (GSE276730), which identified EAAT2 as a high-confidence target (Supporting information Fig. S20). The construction process and key bioinformatic predictions were provided in the Supporting information Table S5−S12. Integration of multiple prediction algorithms identified miR-149-3p as a candidate interacting with both circUnc79 and the glutamate transporter EAAT2 (Fig. 5A). *In vivo* qPCR in morphine-conditioned mice revealed decreased EAAT2 expression ($P < 0.05$) and increased levels of miR-149-3p ($P < 0.01$), consistent with canonical ceRNA interactions (Fig. 5B). Parallel experiments in female mice replicated these expression patterns, confirming sex-independent regulation (Supporting information Fig. S21). After a 28-day withdrawal period, circUnc79 and miR-149-3p returned to baseline levels, while EAAT2 remained elevated compared to controls (Supporting information Fig. S22).

In CATH.a and Neuro-2a cell lines, circUnc79 overexpression reduced miR-149-3p ($P < 0.001$) and elevated EAAT2 mRNA (*Slc1a2*) and protein expression, while circUnc79 knockdown reversed these effects (Fig. 5C−E). Transfection with miR-149-3p mimics suppressed *Slc1a2* level, whereas miR-149-3p inhibitors increased *Slc1a2* level ($P < 0.05$ in CATH.a; $P < 0.01$ in Neuro-2a; Fig. 5F and G). Cross-species sequence analysis demonstrated the evolutionarily conserved miR-149-3p seed complementarity to both circUnc79 and the *Slc1a2*-201 3′ UTR (Fig. 5H).

BaseScope combined with immunofluorescence demonstrated that circUnc79 and AGO2 signals were highly overlapping, supporting its role as a miRNA sponge (Fig. 5I). RNA immunoprecipitation (RIP) assays using an anti-AGO2 antibody enriched circUnc79, miR-149-3p, and *Slc1a2* mRNA relative to IgG controls (Fig. 5J). Dual-luciferase reporter vectors containing wild-type (WT) or mutated (MUT) miR-149-3p binding sites were constructed in the pmirGLO vector (Supporting information Fig. S23) and validated by Sanger sequencing (Fig. 5K and

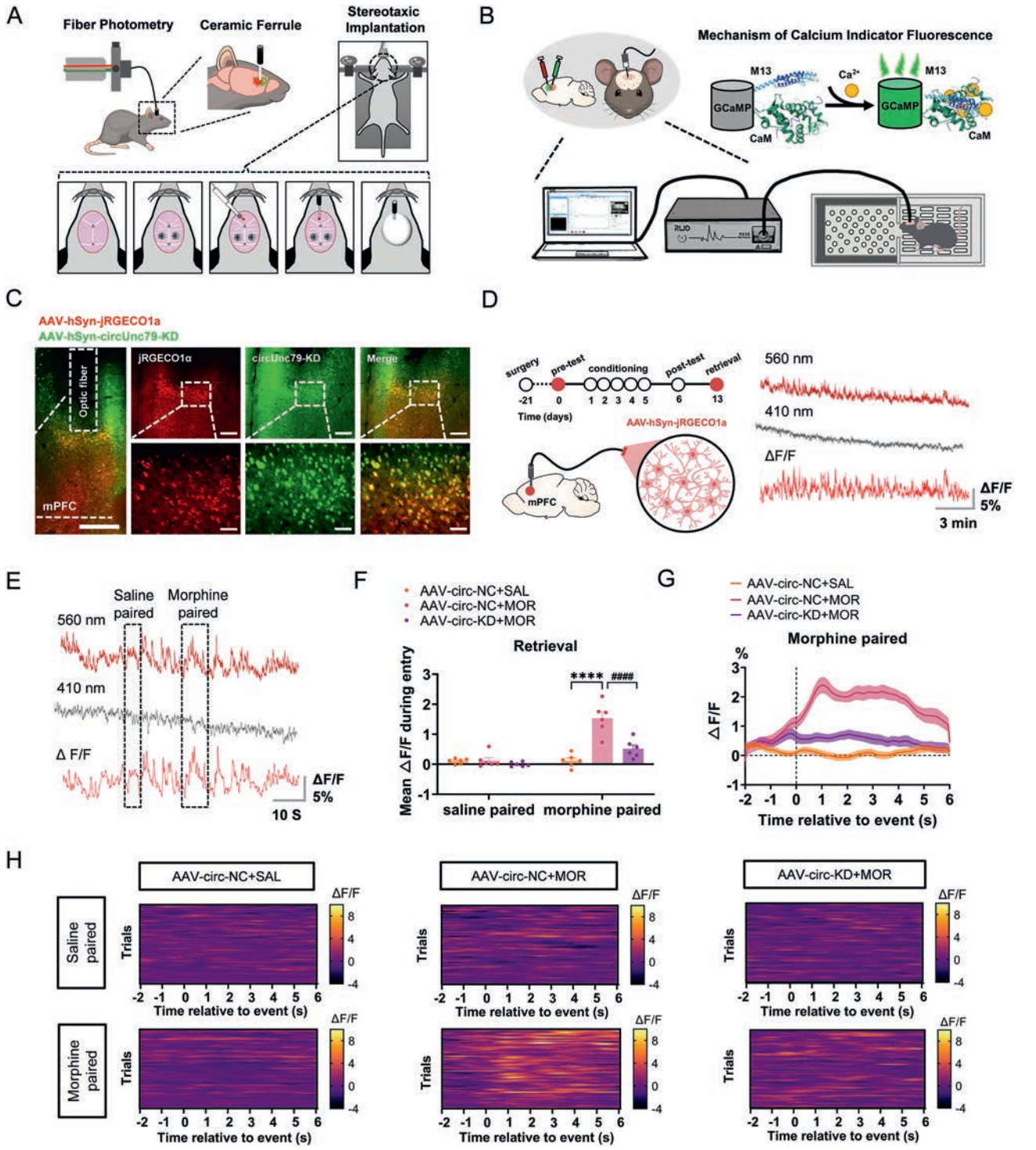

Figure 4 Calcium dynamics revealed circUnc79 effects on neuronal excitability in the mPFC. (A) Procedure for stereotaxic implantation of the optical fiber ferrule. (B) Fiber photometry system and schematic of Ca^{2+}-dependent fluorescence detection. (C) Fluorescence validation of co-expression of AAV-hSyn-JRGECO1a (red) and AAV-hSyn-circUnc79-KD (green) in the mPFC. Scale bars = 500 μm (left), 200 μm (top), 50 μm (bottom). (D) Timeline of fiber photometry recordings and representative calcium traces during CPP testing; normalized $\Delta F/F$ (560 nm) relative to 410 nm reference signals. (E) Event-locked calcium dynamics during chamber transitions; dashed boxes indicated entries into morphine- or saline-paired compartments. (F, G) Quantification of neuronal calcium transient amplitude during chamber entries ($n = 6$). (H) Heatmap of calcium signals aligned to chamber entry events (−2 to +6 s). Each row represented an individual entry event (60 total events from 6 mice). Color intensity reflected normalized $\Delta F/F$. Data are presented as mean ± SEM. $^{****}P < 0.0001$; $^{\#\#\#\#}P < 0.0001$; ns, not significant (one-way ANOVA followed by Bonferroni *post hoc* test).

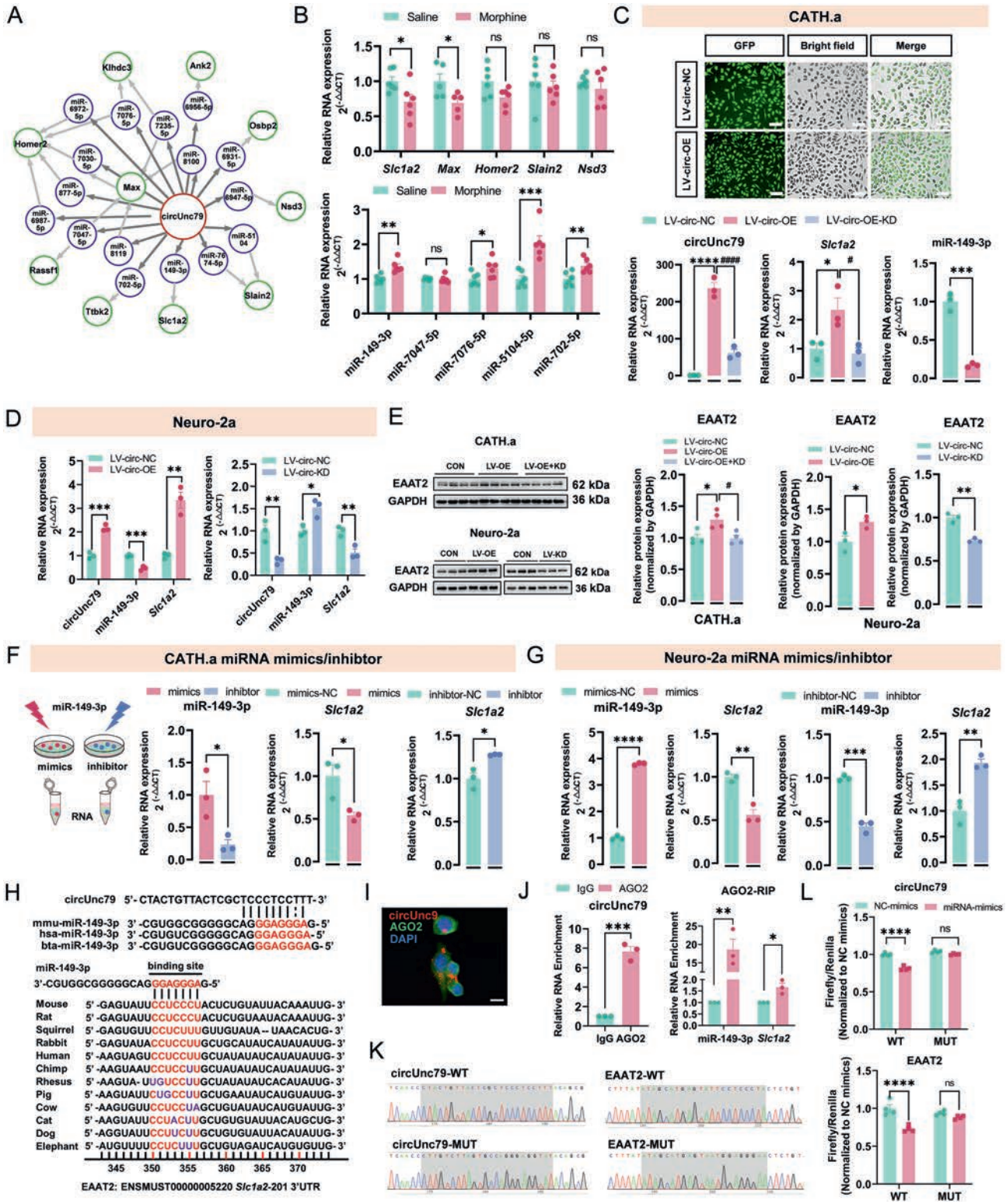

Figure 5 Identification and validation of the circUnc79-mediated ceRNA network. (A) Cytoscape visualization of the circUnc79/miRNA/mRNA network. (B) RT-qPCR validation of reciprocal regulation of the miR-149-3p/EAAT2 axis ($n = 5-6$) (Student's *t*-test). (C) Lentiviral manipulation in CATH.a cells: fluorescence validation of circUnc79 overexpression (top) and corresponding regulation of miR-149-3p and EAAT2 (bottom) ($n = 3$) (Student's *t*-test or one-way ANOVA followed by Bonferroni *post hoc* test). (D, E) Gain- and loss-of-function assays in Neuro-2a cells showing miR-149-3p/EAAT2 regulation (D) and EAAT2 protein levels (E) ($n = 3$) (Student's *t*-test or one-way ANOVA followed by Bonferroni *post hoc* test). (F, G) Functional modulation of miR-149-3p in CATH.a and Neuro-2a cells and its effects on EAAT2 expression ($n = 3$) (Student's *t*-test). (H–J) Predicted binding sites (H), cytoplasmic co-localization of circUnc79 with AGO2 (I), and AGO2-RIP followed by RT-qPCR showing co-enrichment of circUnc79, miR-149-3p, and EAAT2 (J) ($n = 3$) (Student's *t*-test). (K, L) Dual-luciferase reporter assay

Supporting information Fig. S24). Luciferase assays confirmed direct interaction, with miR-149-3p mimics suppressing wild-type reporter activity ($P < 0.0001$), but showing no effect on mutated constructs ($P = 0.87$ *vs.* controls) (Fig. 5L and Supporting information Fig. S25). These findings established circUnc79 as a functional miRNA sponge that sequestered miR-149-3p, thereby relieving translational repression of EAAT2 and linking circUnc79 to glutamatergic signaling regulation.

3.6. miR-149-3p as a functional mediator of circUnc79-dependent morphine reward memory

To clarify the role of miR-149-3p in the circUnc79/miR-149-3p/EAAT2 axis, we manipulated its expression in the mPFC during morphine-induced CPP (Fig. 6A). Microinjection of AgomiR-149-3p resulted in a 1.7-fold increase in mature miR-149-3p levels ($P < 0.001$; Fig. 6B) and impaired both the acquisition and retrieval of reward memory (Fig. 6C), as evidenced by reduced CPP scores ($P < 0.0001$) and decreased preference for the morphine-paired chamber (Fig. 6D). Locomotor activity remained unaffected, confirming behavioral specificity (Fig. 6E).

Conversely, neuron-specific miR-149-3p knockdown *via* adeno-associated virus (Fig. 6F) reduced its expression by 54.28% in the mPFC ($P < 0.01$; Fig. 6G) and enhanced CPP scores during retrieval ($P < 0.05$ *vs.* AAV-miR-NC + MOR; Fig. 6H), without affecting locomotor activity (Fig. 6I). Trajectory heatmaps and 3D reconstructions showed that miR-149-3p-deficient mice increased preference for the drug-paired chamber (Fig. 6J), while general cognitive and exploratory behaviors remained unchanged (Supporting information Fig. S26).

To further examine the circUnc79/miR-149-3p interplay, dual AAV vectors targeting both molecules were co-injected into the mPFC (Fig. 6K). Remarkably, miR-149-3p knockdown reversed the suppressive effect of circUnc79 knockdown on CPP scores ($P < 0.05$; Fig. 6L), restoring chamber preference to morphine control levels (Fig. 6M). Locomotor parameters remained unchanged (Fig. 6N). These bidirectional manipulations demonstrated that miR-149-3p acted as a functional mediator regulated by circUnc79 in opioid reward memory. The rescue of circUnc79 knockdown effects by miR-149-3p deficiency supported a model in which circUnc79 maintained drug-context associations by antagonizing miR-149-3p, linking ceRNA network dynamics to synaptic plasticity.

3.7. The circUnc79/miR-149-3p/EAAT2 axis regulates morphine reward memory via neuronal excitability and glutamatergic homeostasis

To link miR-149-3p′s behavioral effects to synaptic and circuit adaptations, we employed fiber photometry with neuron-specific expression of the calcium indicator jGCaMP7f and miR-149-3p-targeting shRNA (Fig. 7A−C). Representative calcium signals recorded upon entry into saline- or morphine-paired chambers are shown in Fig. 7D. Morphine-treated mice displayed significantly higher mean $\Delta F/F$ upon entering the drug-paired chamber compared to saline controls ($P < 0.0001$; Fig. 7E). Notably, miR-149-3p knockdown further increased mean $\Delta F/F$ ($P < 0.0001$ *vs.* morphine controls). Heatmap analysis confirmed that calcium transients were selectively increased during exploration of the morphine-paired context (Fig. 7F). Event-parameter analysis revealed that memory retrieval significantly increased calcium event frequency ($P < 0.0001$) while decreasing event duration ($P < 0.0001$). Moreover, miR-149-3p knockdown further enhanced event frequency ($P < 0.01$) without altering duration (Supporting information Fig. S27).

To investigate presynaptic adaptations, we employed the glutamate sensor iGluSnFR3.v857 co-expressed with miR-149-3p-targeting shRNA in mPFC neurons (Fig. 7G). The experimental timeline and representative iGluSnFR3.v857 signals were shown in Fig. 7H and I, with representative traces recorded during chamber entry shown in Fig. 7J. Morphine conditioning significantly increased mean glutamate release ($\Delta F/F$) in the mPFC during memory retrieval compared to saline controls ($P < 0.001$). Importantly, miR-149-3p knockdown further potentiated this glutamate release selectively in the morphine-paired chamber (Fig. 7K−M). Kinetic analysis showed that morphine exposure increased release frequency ($P < 0.01$) and shortened the duration ($P < 0.01$), while miR-149-3p knockdown elevated release amplitude without further altering frequency or duration (Supporting information Fig. S28).

To explore how the circUnc79/miR-149-3p/EAAT2 axis regulated synaptic glutamate homeostasis, we isolated synaptosomes from the mPFC following behavioral testing (Fig. 8A and B). Enrichment was validated by increased levels of VGLUT1, PSD95, NMDAR, AMPAR (GluR2), and EAAT2 (Fig. 8C). Western blot analysis revealed that morphine reduced synaptic EAAT2 levels ($P < 0.01$ *vs.* saline), an effect exacerbated by circUnc79 knockdown ($P < 0.05$ *vs.* morphine; Fig. 8D). Concurrently, morphine upregulated synaptic proteins including PSD95 ($P < 0.01$), VGLUT1 ($P < 0.01$) and SYP ($P < 0.001$), which returned to baseline following circUnc79 knockdown ($P < 0.05$ *vs.* morphine; Fig. 8D). Notably, EAAT2 downregulation in the non-synaptosomal fraction induced by morphine was not reversed by circUnc79 knockdown (Supporting information Fig. S29), indicating synapse-specific regulation. Functional epistasis experiments showed that miR-149-3p knockdown restored EAAT2 expression ($P < 0.05$ *vs.* morphine) and further increased VGLUT1 ($P < 0.05$; Fig. 8E). Combined knockdown of circUnc79 and miR-149-3p rescued EAAT2 and VGLUT1 to morphine-treated control levels ($P < 0.05$ *vs.* AAV-circ-KD + MOR; Fig. 8F), establishing miR-149-3p as the key effector of circUnc79 in glutamate homeostasis.

Integrating these molecular and functional data, we proposed that during morphine reward memory retrieval, mPFC neurons exhibited increased excitability supported by enhanced presynaptic glutamate loading and postsynaptic structural potentiation (Fig. 8G). Knockdown of circUnc79 engaged a miR-149-3p-mediated pathway that suppressed synaptic EAAT2 expression, reducing presynaptic glutamate reuptake and potentially affecting VGLUT1-mediated vesicular repackaging and glutamate release. These findings established circUnc79 as a critical regulator coordinating miR-149-3p-dependent neuronal excitability and glutamatergic homeostasis involved in persistent opioid-associated memory.

showing WT and MUT miR-149-3p binding sites and suppression of WT reporter activity by miR-149-3p mimics ($n = 4$) (Student's *t*-test). Scale bars = 100 μm (C), 10 μm (I). Data are presented as mean ± SEM. $^{*}P < 0.05$, $^{**}P < 0.01$, $^{***}P < 0.001$, $^{****}P < 0.0001$; $^{\#}P < 0.05$, $^{\#\#\#\#}P < 0.0001$; ns, not significant.

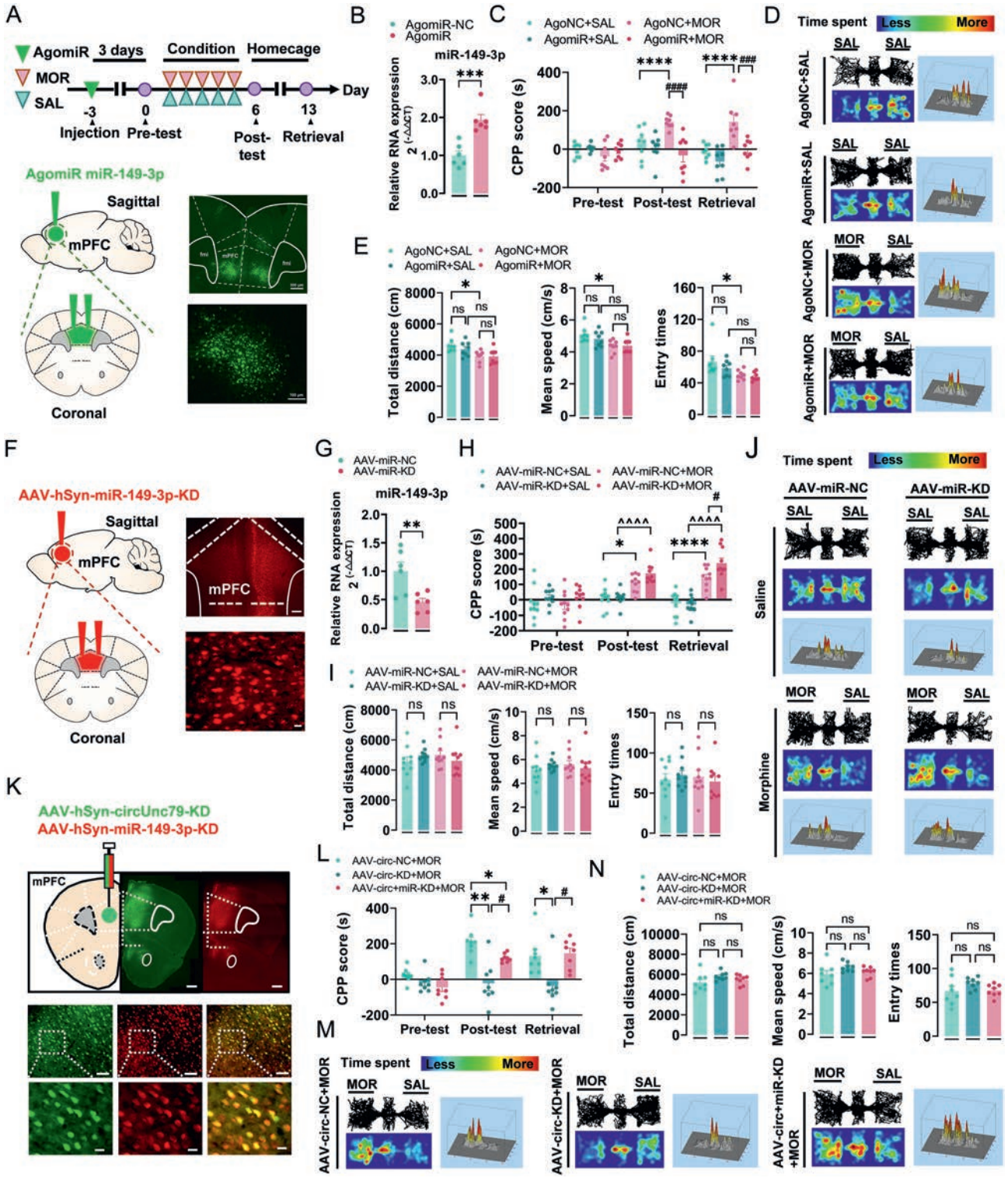

Figure 6 Bidirectional modulation of morphine reward memory by miR-149-3p and rescue of circUnc79 knockdown-induced CPP suppression. (A−E) miR-149-3p AgomiR attenuated morphine reward memory: experimental timeline and fluorescence validation (A), RT-qPCR confirming miR-149-3p upregulation (B), reduced CPP scores during post-test and retrieval (C), representative trajectories and heat maps showing decreased chamber preference (D), and unchanged locomotor activity (E) (n = 7−8) (two-way ANOVA followed by Bonferroni post-hoc test). (F−J) Neuron-specific miR-149-3p knockdown enhanced morphine reward memory: infection validation (F), reduced miR-149-3p levels (G), increased CPP scores without affecting locomotor activity (H, I), and representative trajectories showing enhanced chamber preference (J) (n = 6−10) (two-way ANOVA followed by Bonferroni *post hoc* test). (K−N) miR-149-3p knockdown rescued circUnc79 knockdown-induced CPP suppression: dual-virus co-injection strategy (K), restoration of CPP scores (L), representative trajectories showing recovered chamber preference (M), and unchanged locomotor activity (N) (n = 8) (one-way ANOVA followed by Bonferroni *post hoc* test). Scale

4. Discussion

4.1. CircUnc79 served as a neuron-enriched regulator in morphine-induced reward memory

CircRNAs have recently emerged as important regulators of neuroplasticity and substance use disorders[19]. In this study, we identified circUnc79 as a novel, neuron-enriched circRNA that modulated morphine-induced reward memory in the mPFC. CircUnc79 exhibited canonical circRNA properties, including high stability and resistance to exonuclease-mediated degradation, as validated by RNase R and Actinomycin D treatments. Its parental gene, *Unc79*, encoded a regulatory subunit of the NALCN channel complex that modulated neuronal excitability by controlling sodium leak currents and resting membrane potential[20]. Importantly, morphine conditioning selectively downregulated circUnc79 in the mPFC without affecting *Unc79* mRNA levels across examined brain regions, indicating post-transcriptional regulation rather than host gene transcription. Subcellularly, circUnc79 localized predominantly in the neuronal cytoplasm and presynaptic terminals. This presynaptic enrichment resembled that of circHomer1, which accumulated at synapses to regulate transmission and experience-dependent plasticity[5,21,22], suggesting circUnc79 participated in synaptic remodeling underlying reward memory.

CircUnc79 showed regional specificity. Downregulation occurred exclusively in the mPFC, with no changes in the NAc, hippocampus, BLA, or VTA. Importantly, this regulation occurred only in behaviorally conditioned mice, not in home-cage morphine-treated controls, indicating memory-dependent rather than purely pharmacological effects[23]. While self-administration models mimic active drug-seeking *via* operant conditioning, the CPP paradigm relies on Pavlovian conditioning to specifically isolate the associative learning process between environmental cues and drug reward[24,25]. Given that the mPFC processes contextual associations[26], CPP enabled precise dissection of drug-context memory traces. All effective morphine doses triggered similar circUnc79 downregulation[27], suggesting a saturable response linked to memory formation rather than a graded dose-response effect.

Bidirectional manipulation supported a causal role for circUnc79. Overexpression of circUnc79 enhanced morphine-induced CPP and impaired extinction, whereas knockdown attenuated memory retrieval, facilitated extinction, and prevented morphine-primed reinstatement. Notably, our initial functional screening employed lentiviral vectors with a ubiquitous CMV promoter (LV-circUnc79-OE), which potentially transduced both neurons and glial cells. However, given the demonstrated neuronal enrichment of endogenous circUnc79, we conducted all subsequent loss-of-function experiments, neuronal morphological analyses, and fiber photometry recordings using AAV vectors driven by the neuron-specific hSyn promoter. This neuron-targeted strategy supported the conclusion that the behavioral and mechanistic phenotypes were primarily neuron-driven. We proposed that the endogenous downregulation of circUnc79 represented a compensatory homeostatic response that limits excessive synaptic excitation. Such a mechanism is analogous to negative-feedback adaptations in addiction neurobiology. For example, in the NAc, chronic drug exposure activates cAMP response element-binding protein (CREB), which in turn upregulates dynorphin expression. This CREB−dynorphin pathway has been shown to attenuate cocaine reward, representing a form of negative-feedback adaptation[28].

The upstream mechanisms governing circUnc79 downregulation remained to be fully elucidated. Since circUnc79 changed independently of *Unc79* mRNA, post-transcriptional mechanisms were likely involved. Existing evidence suggested that opioid exposure remodeled the landscape of RNA-binding proteins (RBPs) downstream of μ-opioid receptor (MOR) signaling[29]. Morphine has been shown to modulate the activity of hnRNPK and other splicing factors[30], which may disrupt circRNA biogenesis or stability. Candidate regulators include RBPs that control circRNA stability[31,32] and splicing factors (*e.g.*, DHX9) that modulate back-splicing[33]. Additionally, epigenetic modifications at the *Unc79* locus could also alter back-splicing[4].

Collectively, these findings suggested that circUnc79 was a stable, evolutionarily conserved, and neuron-enriched circRNA that functioned as a spatially and temporally regulated epigenetic modulator of morphine-induced neuroadaptations. Its independence from linear transcript regulation, strategic presynaptic localization, and selective behavioral effects position circUnc79 as a potential therapeutic target for OUD.

4.2. CircUnc79 modulated morphine-induced reward memory via ceRNA network

The circRNA/miRNA/mRNA regulatory axis has emerged as a central mechanism of synaptic plasticity and addiction-related neuroadaptations[7]. CircRNAs can function as ceRNAs that sponge specific miRNAs, thereby influencing downstream mRNA targets essential for synaptic remodeling and drug-seeking behaviors[9]. Here, we identified the circUnc79/miR-149-3p/EAAT2 axis as a previously unrecognized pathway in morphine-induced reward memory.

Our findings demonstrated that circUnc79 functions as a molecular sponge for miR-149-3p, relieving its inhibitory effect on EAAT2 (also known as GLT-1), a transporter essential for maintaining synaptic glutamate homeostasis[11,34]. This ceRNA-mediated regulation was validated through miRNA mimics/inhibitors, dual-luciferase reporter assays, and RIP, confirming that circUnc79 indirectly promoted EAAT2 expression by sequestering miR-149-3p. Bioinformatic analysis revealed that the back-splicing junction of circUnc79 was highly conserved across mammals. Furthermore, the miR-149-3p seed match within the EAAT2 3′ UTR exhibited high conservation between mice and humans, supporting evolutionary preservation of this regulatory module. Although miR-149-3p has been primarily studied in cancer[35], its role in addiction neurobiology has remained largely unexplored. We observed that miR-149-3p specifically modulated the retrieval of morphine-induced CPP. Overexpression impaired retrieval, while knockdown enhanced it. Importantly, both behavioral and molecular responses were conserved across sexes, as female mice displayed similar patterns of the circUnc79/miR-

bars = 300 μm (top), 100 μm (bottom) (A); 200 μm (up), 50 μm (bottom) (F); 500 μm (up), 100 μm (middle), 20 μm (bottom) (K). Data are presented as mean ± SEM. $^{*}P < 0.05$, $^{**}P < 0.01$, $^{***}P < 0.001$, $^{****}P < 0.0001$; $^{\#}P < 0.05$, $^{\#\#\#}P < 0.001$, $^{\#\#\#\#}P < 0.0001$; $^{\hat{}\hat{}\hat{}\hat{}}P < 0.0001$; ns, not significant.

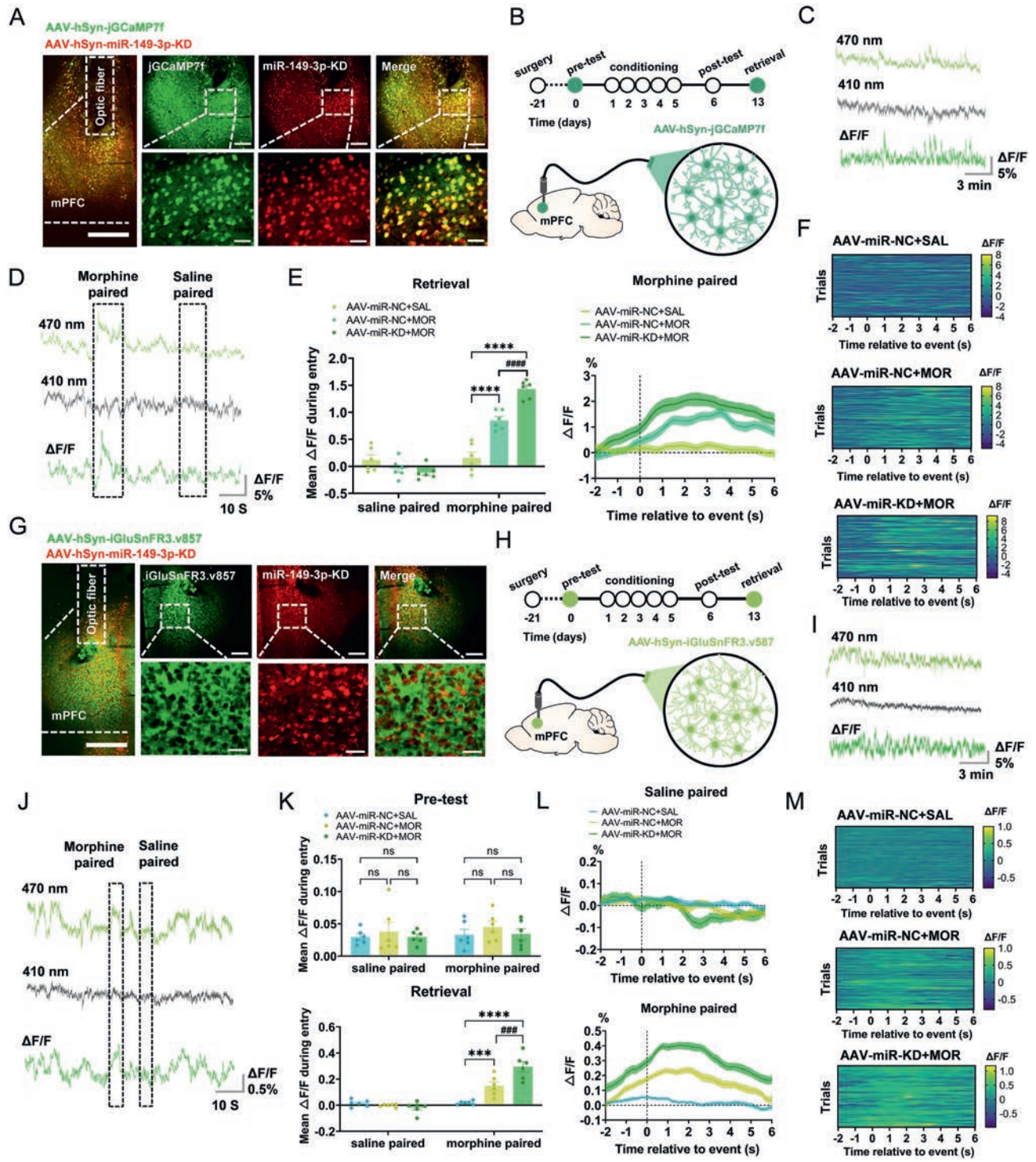

Figure 7 Knockdown of miR-149-3p exacerbated morphine-induced neuronal hyperactivation and glutamate release in the mPFC. (A−F) miR-149-3p deficiency amplified morphine-evoked calcium signaling: co-expression of AAV-hSyn-jGCaMP7f and AAV-hSyn-miR-149-3p-KD in the mPFC (A), fiber photometry recording timeline during CPP (B), representative calcium traces (C), event-locked calcium dynamics during chamber entries (D), increased mean $\Delta F/F$ and increased neuronal activity during entry into the morphine-paired chamber (E), and corresponding heat maps aligned to chamber entry (−2 to +6 s) (F), ($n = 6$) (one-way ANOVA followed by Bonferroni *post hoc* test). (G−M) miR-149-3p knockdown potentiated morphine-associated glutamate release: co-expression of AAV-hSyn-iGluSnFR3.v857 and AAV-miR-149-3p-KD in the mPFC (G), recording timeline synchronized with CPP phases (H), representative glutamate signal traces (I), event-aligned glutamate dynamics during chamber entries (J), increased $\Delta F/F$ during entry into the morphine-paired chamber (K), real-time glutamate dynamics during saline- and morphine-paired chamber entries (L), and corresponding heat maps aligned to morphine-paired chamber entry (−2 to +6 s) (M) ($n = 6$) (one-way ANOVA followed by Bonferroni *post hoc* test). Scale bars = 500 μm (left), 200 μm (top), 50 μm (bottom) in panels A and G. Data are presented as mean ± SEM. $^{***}P < 0.001$, $^{****}P < 0.0001$; $^{\#\#\#}P < 0.001$, $^{\#\#\#\#}P < 0.0001$; ns, not significant.

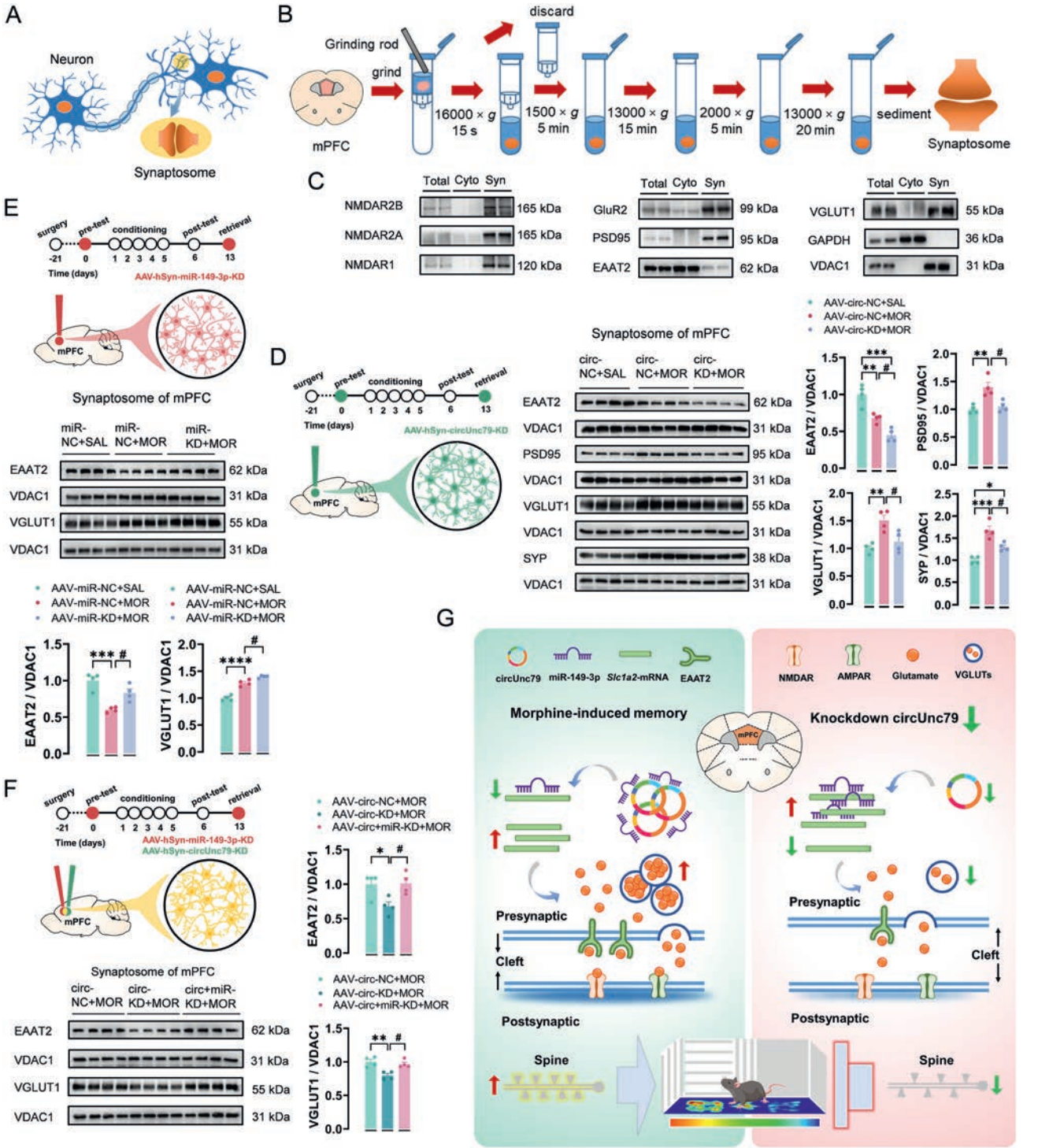

Figure 8 Synaptosome profiling revealed the function of the circUnc79/miR-149-3p/EAAT2 axis in morphine-induced memory retrieval. (A−C) Synaptosome isolation and validation from the mPFC: schematic of synaptic structures in mPFC tissue (A), synaptosome enrichment workflow (B), and Western blotting validation showing enrichment of synapse-associated proteins in isolated synaptosomes (C). (D−F) Regulation of synaptosomal proteins by the circUnc79/miR-149-3p axis. (D) Knockdown of circUnc79 altered synapse-associated protein levels in synaptosomes during morphine reward memory retrieval ($n = 4$). (E) Synaptosome Western blotting analysis revealed that miR-149-3p knockdown increased EAAT2 and VGLUT1 expression ($n = 4$). (F) Knockdown of miR-149-3p reversed circUnc79 knockdown-induced alterations in synaptosomal EAAT2 and VGLUT1 during morphine reward memory retrieval ($n = 4$). (G) Proposed model illustrating the role of circUnc79 in regulating morphine reward memory through the miR-149-3p/EAAT2 axis. During memory retrieval, circUnc79 knockdown activated a miR-149-3p-dependent pathway, resulting in reduced neuronal EAAT2 expression and altered VGLUT1-associated glutamatergic transmission and synaptic plasticity, thereby modulating morphine reward memory retrieval. Data are presented as mean ± SEM. $^{*}P < 0.05$, $^{**}P < 0.01$, $^{***}P < 0.001$, $^{****}P < 0.0001$; $^{\#}P < 0.05$; ns, not significant.

149-3p/EAAT2 axis, supporting the therapeutic relevance of this axis.

EAAT2 is the principal glutamate transporter in the CNS, responsible for clearing 80%−90% of extracellular glutamate[15]. Although EAAT2 is predominantly localized to astrocytes, it has also been reported in neurons and synaptic fractions, including presynaptic compartments[12]. Our synaptosomal analysis confirmed EAAT2 presence in mPFC neuronal synapses (Fig. 8C), suggesting a neuron-specific mechanism through which circUnc79 regulated glutamatergic signaling. Dysregulated glutamatergic transmission is a core feature of addiction pathology, with EAAT2 acting as a critical homeostatic regulator[36]. Chronic drug exposure typically downregulates EAAT2, impairing glutamate clearance and promoting synaptic hyperexcitability[37,38]. While previous studies focused on astrocytic EAAT2, our results demonstrated that the retrieval of morphine reward memory was accompanied by a significant reduction of EAAT2 specifically in mPFC synaptosomes.

Neuronal EAAT2 knockout models supported this distinction[13,14]. Deletion of neuronal EAAT2 disrupted glutamate uptake at synaptic terminals, triggering compensatory astrocyte-to-neuron glutamine transfer[14]. Despite such compensation, these mice exhibited normal baseline behaviors but significantly altered responses to psychostimulants[39], implying a specialized role for neuronal EAAT2 in modulating circuit sensitivity to drugs of abuse. Consistent with this, circUnc79 knockdown reduced presynaptic EAAT2 expression in the mPFC, likely disrupting glutamatergic homeostasis during reward memory retrieval by shifting the excitatory balance within local mPFC microcircuits[40].

Temporal analysis revealed critical stage-specific regulation. During early retrieval, the circUnc79/miR-149-3p/EAAT2 axis was significantly dysregulated. However, following 28 days of protracted withdrawal, both circUnc79 and miR-149-3p normalized to baseline, while EAAT2 expression rebounded above control levels. This temporal dissociation suggested that the ceRNA axis specifically governed memory retrieval, whereas persistent EAAT2 upregulation during long-term abstinence reflected compensatory homeostatic adaptation driven by alternative mechanisms. This distinction suggested a potential therapeutic window for targeting the circUnc79 axis during early withdrawal and retrieval, distinct from mechanisms maintaining protracted abstinence.

Our results suggested the therapeutic potential of this axis through bidirectional interventions. CircUnc79 overexpression impaired extinction learning, rendering reward memories resistant to suppression. Conversely, AAV-mediated circUnc79 knockdown facilitated extinction training and abolished morphine priming-induced reinstatement. Since relapse prevention remains the most challenging aspect of OUD treatment, the ability of circUnc79 downregulation to disrupt pathological reward associations and confer lasting protection against reinstatement positions it as a promising candidate.

While this study focused on morphine, the circUnc79/miR-149-3p/EAAT2 axis likely extended to other opioids. Morphine, heroin, and fentanyl all activate μ-opioid receptors and share overlapping intracellular signaling cascades[41], and EAAT2 downregulation has been documented across multiple addictive substances[42]. In summary, while the loss of neuronal EAAT2 might not compromise basal function, its dynamic regulation by the circUnc79/miR-149-3p axis proved essential for the encoding and persistence of pathological drug memories.

4.3. CircUnc79 orchestrated morphine-induced synaptic remodeling in the mPFC

Synaptic plasticity underlies memory encoding and stabilization, particularly in addiction-related memory circuits such as the mPFC[43]. In this study, we identified circUnc79 as a critical regulator of morphine-induced synaptic remodeling, coordinating structural and functional adaptations through the miR-149-3p/EAAT2 axis. Morphologically, chronic morphine exposure increased dendritic complexity and selectively enhanced mushroom spine density in mPFC neurons, consistent with long-term potentiation (LTP) and memory consolidation[44]. Concomitant reduction in thin spine density suggested redistribution toward more stable synaptic configurations, supporting the formation of enduring drug-associated memories[23,45]. Importantly, circUnc79 knockdown reversed these adaptations, underscoring its necessity for morphine-induced structural plasticity[17,46].

At the ultrastructural level, retrieval of reward memory induced synaptic modifications characterized by increased presynaptic vesicle density, thickened postsynaptic density (PSD), and narrowed synaptic clefts, collectively indicating enhanced synaptic efficacy. These structural alterations were accompanied by upregulation of key synaptic proteins: PSD95 facilitated glutamate receptor anchoring[47], while VGLUT1 and SYP supported glutamate packaging and vesicle trafficking[48,49]. CircUnc79 knockdown normalized these parameters, revealing its dual role in presynaptic vesicle dynamics and postsynaptic receptor organization[50].

Functionally, fiber photometry recordings revealed that retrieval of drug-associated memories triggered circuit hyperexcitability[51,52]. Knockdown of circUnc79 significantly attenuated this hyperexcitability. Although AAV-mediated knockdown was initiated prior to CPP training, retrieval-phase measurements remained critical for assessing circuit dysfunction. Event-parameter analysis revealed that retrieval shifted activity toward a more "burst-like" pattern. Parallel recordings using the glutamate sensor iGluSnFR3.v857 showed exaggerated glutamate transients upon re-exposure to drug context, consistent with presynaptic glutamate dysregulation that drove postsynaptic calcium hyperactivity. Mechanistically, circUnc79 knockdown normalized these burst patterns and restored glutamate release kinetics, whereas miR-149-3p knockdown exacerbated them, confirming a hierarchical regulatory relationship. Collectively, morphine conditioning induced an adaptive downregulation of neuronal EAAT2, while circUnc79 knockdown further increased miR-149-3p availability, leading to miR-149-3p-mediated inhibition of presynaptic EAAT2 and effectively suppressing reward memory retrieval. Notably, these manipulations altered glutamate dynamics without inducing anxiety- or depression-like behaviors, suggesting that the circUnc79/miR-149-3p/EAAT2 axis selectively regulated addiction-related plasticity rather than baseline emotional processing[53].

We further elucidated the coupling between VGLUT1 and EAAT2. Neuronal EAAT2 localized to presynaptic terminals where it recycled glutamate for vesicular repackaging[12−14]. Our data suggested that circUnc79 regulated VGLUT1 indirectly through metabolic coupling with EAAT2. Functionally, presynaptic EAAT2 was essential for replenishing the cytoplasmic glutamate pool required for neurotransmitter resynthesis[10,12,48]. We proposed that the adaptive downregulation of neuronal EAAT2 in morphine-conditioned mice triggered compensatory VGLUT1 reduction to match substrate availability. This coupling was supported by pharmacological studies showing ceftriaxone-mediated

EAAT2 upregulation restored VGLUT1 expression[54], and by our rescue experiments demonstrating miR-149-3p inhibition normalized both EAAT2 and VGLUT1 levels. Beyond vesicular loading, EAAT2 modulated AMPAR trafficking and LTP-like plasticity during cue-induced drug seeking[55,56], influencing calcium dynamics that governed spine morphogenesis[57] and PSD organization[58]. Thus, circUnc79 maintained presynaptic glutamate homeostasis by stabilizing EAAT2, which supported VGLUT1-dependent vesicular loading.

Although clinical data on circUnc79 remain limited, therapeutic validity of the EAAT2 pathway is well-established. Postmortem studies documented reduced EAAT2 in the prefrontal cortex of individuals with substance use disorders[59], and *N*-acetylcysteine demonstrated efficacy for reducing craving in clinical trials[60,61]. Unlike systemic agents with limited specificity[62,63], circUnc79-based approaches could selectively normalize glutamate dynamics in addiction circuits *via* the ceRNA mechanism. The translational potential of circUnc79 is further supported by favorable drug-like properties. Its circular structure confers exonuclease resistance, enabling sustained therapeutic effects. Multiple delivery platforms have been clinically validated, including AAV vectors with favorable safety profiles in neurological clinical trials[64] and FDA-approved antisense oligonucleotides (ASOs) like nusinersen[65]. Emerging non-viral platforms, such as extracellular vesicles[66] and lipid nanoparticles (LNPs)[67], promise efficient blood−brain barrier penetration with reduced immunogenicity[68]. Future efforts should optimize CNS tropism and assess long-term safety to advance circRNA-based precision medicine for addiction treatment.

5. Conclusions

In conclusion, we identified circUnc79 as a neuron-enriched regulator that coordinates morphine-induced synaptic remodeling through the circUnc79/miR-149-3p/EAAT2 axis. By integrating presynaptic glutamate recycling with postsynaptic structural plasticity, circUnc79 links noncoding RNA biology to addiction-related neuroadaptations. Collectively, our findings demonstrate that circUnc79 is a key epigenetic mediator of opioid reward and a potential therapeutic target for opioid use disorder.

Data availability

Data supporting the findings of this study were included in the article and its Supporting Information. Raw and processed high-throughput sequencing data were deposited in the NCBI Gene Expression Omnibus under accession numbers GSE221797 and GSE276730.

Acknowledgments

We thank all the members of our laboratory for helpful discussions and the Center of Analysis and Testing of Xi'an Jiaotong University for technical support. This work was supported by the Open Project of Shaanxi Key Laboratory of Drug Analysis and Intelligent Monitoring (NNLS-0-202309, China), the Natural Science Basic Research Program of Shaanxi Province (2024JC-YBMS-634, China), the Fundamental Research Funds for the Central Universities of Xi'an Jiaotong University (xzy022024029, xzy022024034 and xzy022025086, China), and the Project of Independent Innovation Experiment for Postgraduates in Medicine in Xi'an Jiaotong University (YJSCX-2026-009, China).

Author contributions

Chunxia Yan and Yuxiang Zhang conceived the study and developed the hypothesis. Xixi Yang conducted the experiments and wrote the draft of the manuscript. Xixi Yang and Feifei Gao analyzed the data and performed the statistical analysis. Zhuojin Yang, Dongyu Yu and Jie Chen contributed to figure preparation. Zhen Yao and Qi Liao checked the data. Jingsi Yang, Junlin Liu and Boyuan Gu assisted with behavioral testing and sample preparation. Chunxia Yan and Yuxiang Zhang supervised the project and revised the manuscript. All authors reviewed and approved the final version of the manuscript.

Conflicts of interest

The authors declare no conflicts of interest.

Appendix A. Supporting information

Supporting information to this article can be found online at https://doi.org/10.1016/j.apsb.2026.06.004.

References

1. Strang J, Volkow ND, Degenhardt L, Hickman M, Johnson K, Koob GF, et al. Opioid use disorder. *Nat Rev Dis Primers* 2020;**6**:3.
2. Milton AL, Everitt BJ. The persistence of maladaptive memory: addiction, drug memories and anti-relapse treatments. *Neurosci Biobehav Rev* 2012;**36**:1119−39.
3. Koob GF, Volkow ND. Neurobiology of addiction: a neurocircuitry analysis. *Lancet Psychiatry* 2016;**3**:760−73.
4. Browne CJ, Godino A, Salery M, Nestler EJ. Epigenetic mechanisms of opioid addiction. *Biol Psychiatry* 2020;**87**:22−33.
5. Rybak-Wolf A, Stottmeister C, Glažar P, Jens M, Pino N, Giusti S, et al. Circular RNAs in the mammalian brain are highly abundant, conserved, and dynamically expressed. *Mol Cell* 2015;**58**:870−85.
6. Dong X, Bai Y, Liao Z, Gritsch D, Liu X, Wang T, et al. Circular RNAs in the human brain are tailored to neuron identity and neuropsychiatric disease. *Nat Commun* 2023;**14**:5327.
7. Hansen TB, Jensen TI, Clausen BH, Bramsen JB, Finsen B, Damgaard CK, et al. Natural RNA circles function as efficient microRNA sponges. *Nature* 2013;**495**:384−8.
8. Zhang Y, Du L, Bai Y, Han B, He C, Gong L, et al. CircDYM ameliorates depressive-like behavior by targeting miR-9 to regulate microglial activation *via* HSP90 ubiquitination. *Mol Psychiatr* 2020; **25**:1175−90.
9. Yu H, Xie B, Zhang J, Luo Y, Galaj E, Zhang X, et al. The role of circTmeff-1 in incubation of context-induced morphine craving. *Pharmacol Res* 2021;**170**:105722.
10. Kalivas PW. The glutamate homeostasis hypothesis of addiction. *Nat Rev Neurosci* 2009;**10**:561−72.
11. Roberts-Wolfe DJ, Kalivas PW. Glutamate transporter GLT-1 as a therapeutic target for substance use disorders. *CNS Neurol Disord: Drug Targets* 2015;**14**:745−56.
12. Rimmele TS, Rosenberg PA. GLT-1: the elusive presynaptic glutamate transporter. *Neurochem Int* 2016;**98**:19−28.
13. McNair LF, Andersen JV, Aldana BI, Hohnholt MC, Nissen JD, Sun Y, et al. Glutamate transporter GLT-1 as a therapeutic target for substance use disorders. *J Neurosci* 2019;**39**:4847−63.
14. McNair LF, Andersen JV, Nissen JD, Sun Y, Fischer KD, Hodgson NW, et al. Conditional knockout of GLT-1 in neurons leads to alterations in aspartate homeostasis and synaptic mitochondrial metabolism in striatum and hippocampus. *Neurochem Res* 2020;**45**:1420−37.

15. Takahashi K, Foster JB, Lin CL. Glutamate transporter EAAT2: regulation, function, and potential as a therapeutic target for neurological and psychiatric disease. *Cell Mol Life Sci* 2015;**72**:3489−506.
16. Yang X, Yu D, Gao F, Yang J, Chen Z, Liu J, et al. Integrative analysis of morphine-induced differential Circular RNAs and ceRNA networks in the medial prefrontal cortex. *Mol Neurobiol* 2024;**61**:4602−18.
17. Yang Z, Yu D, Gao F, Zhou D, Wu Y, Yang X, et al. The histone lysine demethylase KDM7A contributes to reward memory *via* Fscn1-induced synaptic plasticity in the medial prefrontal cortex. *Adv Sci (Weinh)* 2025;**12**:e2405352.
18. Yang X, Wen Y, Zhang Y, Gao F, Yang J, Yang Z, et al. Dynamic changes of cytoskeleton-related proteins within reward-related brain regions in morphine-associated memory. *Front Neurosci* 2020;**14**: 626348.
19. Daws SE, Gillespie A. Circular RNA regulation and function in drug seeking phenotypes. *Mol Cell Neurosci* 2023;**125**:103841.
20. Kschonsak M, Chua HC, Weidling C, Chakouri N, Noland CL, Schott K, et al. Structural architecture of the human NALCN channelosome. *Nature* 2022;**603**:180−6.
21. Zimmerman AJ, Hafez AK, Amoah SK, Rodriguez BA, Dell'Orco M, Lozano E, et al. A psychiatric disease-related circular RNA controls synaptic gene expression and cognition. *Mol Psychiatr* 2020;**25**: 2712−27.
22. You X, Vlatkovic I, Babic A, Will T, Epstein I, Tushev G, et al. Neural circular RNAs are derived from synaptic genes and regulated by development and plasticity. *Nat Neurosci* 2015;**18**:603−10.
23. Fakira AK, Massaly N, Cohensedgh O, Berman A, Morón JA. Morphine-associated contextual cues induce structural plasticity in hippocampal CA1 pyramidal neurons. *Neuropsychopharmacology* 2016;**41**:2668−78.
24. Hyman SE, Malenka RC, Nestler EJ. Neural mechanisms of addiction: the role of reward-related learning and memory. *Annu Rev Neurosci* 2006;**29**:565−98.
25. Bardo MT, Bevins RA. Conditioned place preference: what does it add to our preclinical understanding of drug reward? *Psychopharmacology (Berl)* 2000;**153**:31−43.
26. Euston DR, Gruber AJ, McNaughton BL. The role of medial prefrontal cortex in memory and decision making. *Neuron* 2012;**76**: 1057−70.
27. Ribeiro Do Couto B, Aguilar MA, Manzanedo C, Rodríguez-Arias M, Miñarro J. Reinstatement of morphine-induced conditioned place preference in mice by priming injections. *Neural Plast* 2003;**10**: 279−90.
28. Carlezon WA, Thome J, Olson VG, Lane-Ladd SB, Brodkin ES, Hiroi N, et al. Regulation of cocaine reward by CREB. *Science* 1998; **282**:2272−5.
29. Song KY, Choi HS, Law P, Wei L, Loh HH. Post-transcriptional regulation of mu-opioid receptor: role of the RNA-binding proteins heterogeneous nuclear ribonucleoprotein H1 and F. *Cell Mol Life Sci* 2011;**69**:599−610.
30. Song KY, Choi HS, Law P, Wei L, Loh HH. Post-transcriptional regulation of the human mu-opioid receptor (MOR) by morphine-induced rna binding proteins hnRNP K and PCBP1. *J Cell Physiol* 2016;**232**:576−84.
31. Conn SJ, Pillman KA, Toubia J, Conn VM, Salmanidis M, Phillips CA, et al. The RNA binding protein quaking regulates formation of circRNAs. *Cell* 2015;**160**:1125−34.
32. Chen LL. The expanding regulatory mechanisms and cellular functions of circular RNAs. *Nat Rev Mol Cell Biol* 2020;**21**:475−90.
33. Aktaş T, Avşar Ilık İ, Maticzka D, Bhardwaj V, Pessoa Rodrigues C, Mittler G, et al. DHX9 suppresses RNA processing defects originating from the alu invasion of the human genome. *Nature* 2017;**544**: 115−9.
34. Bjørnsen LP, Hadera MG, Zhou Y, Danbolt NC, Sonnewald U. The GLT-1 (EAAT2; slc1a2) glutamate transporter is essential for glutamate homeostasis in the neocortex of the mouse. *J Neurochem* 2014; **128**:641−9.
35. Cao Y, Wang Z, Yan Y, Ji L, He J, Xuan B, et al. Enterotoxigenic bacteroidesfragilis promotes intestinal inflammation and malignancy by inhibiting exosome-packaged miR-149-3p. *Gastroenterology* 2021; **161**:1552−66.e12.
36. Scofield MD, Kalivas PW. Astrocytic dysfunction and addiction: consequences of impaired glutamate homeostasis. *Neuroscientist* 2014;**20**:610−22.
37. Kim R, Sepulveda-Orengo MT, Healey KL, Williams EA, Reissner KJ. Regulation of glutamate transporter 1 (GLT-1) gene expression by cocaine self-administration and withdrawal. *Neuropharmacology* 2018;**128**:1−10.
38. Saeedi N, Darvishmolla M, Tavassoli Z, Davoudi S, Heysieattalab S, Hosseinmardi N, et al. The role of hippocampal glial glutamate transporter (GLT-1) in morphine-induced behavioral responses. *Brain Behav* 2021;**11**:e2323.
39. Fischer KD, Houston ACW, Desai RI, Doyle MR, Bergman J, Mian M, et al. Behavioral phenotyping and dopamine dynamics in mice with conditional deletion of the glutamate transporter GLT-1 in neurons: resistance to the acute locomotor effects of amphetamine. *Psychopharmacology (Berl)* 2018;**235**:1371−87.
40. Jiang C, Wang X, Le Q, Liu P, Liu C, Wang Z, et al. Morphine coordinates SST and PV interneurons in the prelimbic cortex to disinhibit pyramidal neurons and enhance reward. *Mol Psychiatr* 2021;**26**: 1178−93.
41. Al-Hasani R, Bruchas MR. Molecular mechanisms of opioid receptor-dependent signaling and behavior. *Anesthesiology* 2011;**115**:1363−81.
42. Spencer S, Kalivas PW. Glutamate transport: a new bench to bedside mechanism for treating drug abuse. *Int J Neuropsychopharmacol* 2017;**20**:797−812.
43. Kauer JA, Malenka RC. Synaptic plasticity and addiction. *Nat Rev Neurosci* 2007;**8**:844−58.
44. Holtmaat A, Svoboda K. Experience-dependent structural synaptic plasticity in the mammalian brain. *Nat Rev Neurosci* 2009;**10**: 647−58.
45. Wang Y, Zhang H, Cui J, Zhang J, Yin F, Guo H, et al. Opiate-associated contextual memory formation and retrieval are differentially modulated by dopamine D1 and D2 signaling in hippocampal-prefrontal connectivity. *Neuropsychopharmacology* 2019;**44**:334−43.
46. Lüscher C, Malenka RC. Drug-evoked synaptic plasticity in addiction: from molecular changes to circuit remodeling. *Neuron* 2011;**69**: 650−63.
47. Wang Z, Yan P, Hui T, Zhang J. Epigenetic upregulation of PSD-95 contributes to the rewarding behavior by morphine conditioning. *Eur J Pharmacol* 2014;**732**:123−9.
48. Martineau M, Guzman RE, Fahlke C, Klingauf J. VGLUT1 functions as a glutamate/proton exchanger with chloride channel activity in hippocampal glutamatergic synapses. *Nat Commun* 2017;**8**:2279.
49. Kravčenko U, Ruwolt M, Kroll J, Yushkevich A, Zenkner M, Ruta J, et al. Molecular architecture of synaptic vesicles. *Proc Natl Acad Sci U S A* 2024;**121**:e2407375121.
50. Otis JM, Mueller D. Reversal of cocaine-associated synaptic plasticity in medial prefrontal cortex parallels elimination of memory retrieval. *Neuropsychopharmacology* 2017;**42**:2000−10.
51. Otis JM, Fitzgerald MK, Yousuf H, Burkard JL, Drake M, Mueller D. Prefrontal neuronal excitability maintains cocaine-associated memory during retrieval. *Front Behav Neurosci* 2018;**12**:119.
52. Zhang T, Yanagida J, Kamii H, Wada S, Domoto M, Sasase H, et al. Glutamatergic neurons in the medial prefrontal cortex mediate the formation and retrieval of cocaine-associated memories in mice. *Addict Biol* 2020;**25**:e12723.
53. Otis JM, Namboodiri VMK, Matan AM, Voets ES, Mohorn EP, Kosyk O, et al. Prefrontal cortex output circuits guide reward seeking through divergent cue encoding. *Nature* 2017;**543**:103−7.
54. Fan S, Li L, Xian X, Liu L, Gao J, Li W. Ceftriaxone regulates glutamate production and vesicular assembly in presynaptic terminals through GLT-1 in APP/PS1 mice. *Neurobiol Learn Mem* 2021;**183**: 107480.

55. Hearing MC, Jedynak J, Ebner SR, Ingebretson A, Asp AJ, Fischer RA, et al. Reversal of morphine-induced cell-type-specific synaptic plasticity in the nucleus accumbens shell blocks reinstatement. *Proc Natl Acad Sci U S A* 2016;**113**:757−62.
56. Spencer S, Garcia-Keller C, Roberts-Wolfe D, Heinsbroek JA, Mulvaney M, Sorrell A, et al. Cocaine use reverses striatal plasticity produced during cocaine seeking. *Biol Psychiatry* 2017;**81**: 616−24.
57. Wang X, Cahill ME, Werner CT, Christoffel DJ, Golden SA, Xie Z, et al. Kalirin-7 mediates cocaine-induced AMPA receptor and spine plasticity, enabling incentive sensitization. *J Neurosci* 2013;**33**: 11012−22.
58. Béïque JC, Lin DT, Kang MG, Aizawa H, Takamiya K, Huganir RL. Synapse-specific regulation of AMPA receptor function by PSD-95. *Proc Natl Acad Sci U S A* 2006;**103**:19535−40.
59. Smaga I, Frankowska M, Filip M. N-acetylcysteine in substance use disorder: a lesson from preclinical and clinical research. *Pharmacol Rep* 2021;**73**:1205−19.
60. Deepmala Slattery J, Kumar N, Delhey L, Berk M, Dean O, et al. Clinical trials of *N*-acetylcysteine in psychiatry and neurology: a systematic review. *Neurosci Biobehav Rev* 2015;**55**:294−321.
61. Chang CT, Hsieh PJ, Lee HC, Lo CH, Tam KW, Loh EW. Effectiveness of *N*-acetylcysteine in treating clinical symptoms of substance abuse and dependence: a meta-analysis of randomized controlled trials. *Clin Psychopharmacol Neurosci* 2021;**19**:282−93.
62. Abulseoud OA, Miller JD, Wu J, Choi DS, Holschneider DP. Ceftriaxone upregulates the glutamate transporter in medial prefrontal cortex and blocks reinstatement of methamphetamine seeking in a condition place preference paradigm. *Brain Res* 2012;**1456**:14−21.
63. Smaga I, Fierro D, Mesa J, Filip M, Knackstedt LA. Molecular changes evoked by the beta-lactam antibiotic ceftriaxone across rodent models of substance use disorder and neurological disease. *Neurosci Biobehav Rev* 2020;**115**:116−30.
64. Mendell JR, Al-Zaidy S, Shell R, Arnold WD, Rodino-Klapac LR, Prior TW, et al. Single-dose gene-replacement therapy for spinal muscular atrophy. *N Engl J Med* 2017;**377**:1713−22.
65. Finkel RS, Mercuri E, Darras BT, Connolly AM, Kuntz NL, Kirschner J, et al. Nusinersen *versus* sham control in infantile-onset spinal muscular atrophy. *N Engl J Med* 2017;**377**:1723−32.
66. Yang L, Han B, Zhang Z, Wang S, Bai Y, Zhang Y, et al. Extracellular vesicle-mediated delivery of circular RNA SCMH1 promotes functional recovery in rodent and nonhuman primate ischemic stroke models. *Circulation* 2020;**142**:556−74.
67. Jia Y, Xu L, Leng S, Sun Y, Huang X, Wang Y, et al. Nose-to-brain delivery of circular RNA SCMH1-loaded lipid nanoparticles for ischemic stroke therapy. *Adv Mater* 2025;**37**:e2500598.
68. Wesselhoeft RA, Kowalski PS, Parker-Hale FC, Huang Y, Bisaria N, Anderson DG. RNA circularization diminishes immunogenicity and can extend translation duration *in vivo*. *Mol Cell* 2019;**74**: 508−20.